Phenotypic changes in mouse pancreatic stellate cell Ca^{2+} signaling events following activation in culture and in a disease model of pancreatitis

Jong Hak Won[a], Yu Zhang[a], Baoan Ji[b], Craig D. Logsdon[b], and David I. Yule[a]
[a]Department of Pharmacology and Physiology, University of Rochester Medical Center, Rochester, NY 14642;
[b]Department of Cancer Biology, University of Texas MD Anderson Cancer Center, Houston, TX 77030

ABSTRACT **The specific characteristics of intracellular Ca^{2+} signaling and the downstream consequences of these events were investigated in mouse pancreatic stellate cells (PSC) in culture and in situ using multiphoton microscopy in pancreatic lobules. PSC undergo a phenotypic transformation from a quiescent state to a myofibroblast-like phenotype in culture. This is believed to parallel the induction of an activated state observed in pancreatic disease such as chronic pancreatitis and pancreatic cancer. By day 7 in culture, the complement of cell surface receptors coupled to intracellular Ca^{2+} signaling was shown to be markedly altered. Specifically, protease-activated receptors (PAR) 1 and 2, responsive to thrombin and trypsin, respectively, and platelet-derived growth factor (PDGF) receptors were expressed only in activated PSC (aPSC). PAR-1, ATP, and PDGF receptor activation resulted in prominent nuclear Ca^{2+} signals. Nuclear Ca^{2+} signals and aPSC proliferation were abolished by expression of parvalbumin targeted to the nucleus. In pancreatic lobules, PSC responded to agonists consistent with the presence of only quiescent PSC. aPSC were observed following induction of experimental pancreatitis. In contrast, in a mouse model of pancreatic disease harboring elevated K-Ras activity in acinar cells, aPSC were present under control conditions and their number greatly increased following induction of pancreatitis. These data are consistent with nuclear Ca^{2+} signaling generated by agents such as trypsin and thrombin, likely present in the pancreas in disease states, resulting in proliferation of "primed" aPSC to contribute to the severity of pancreatic disease.**

Monitoring Editor
M. Bishr Omary
University of Michigan

Received: Oct 7, 2010
Revised: Nov 15, 2010
Accepted: Nov 30, 2010

INTRODUCTION

The primary physiological role of the exocrine pancreas is to produce pancreatic juice—an important conduit for the initial digestion of ingested nutrients in the small intestine. Neural and hormonal stimulation of the exocrine pancreas following a meal results in the production of a fluid rich in HCO_3^- and containing a complex mixture of proteins (Williams and Yule, 2006). The proteins are predominately inactive precursors of digestive enzymes that are subsequently activated in the lumen of the duodenum. Two epithelial cell types are primarily responsible for secretion from the gland. Acinar cells synthesize, store, and undergo regulated exocytosis of secretory granules while duct cells are responsible for the aqueous component of the secretion. Together, these cells result in the formation and delivery of pancreatic juice to the duodenum. A third, less studied cell type, pancreatic stellate cells (PSC), are also resident in the exocrine pancreas. PSC are present in a periacinar and periductal localization (Apte *et al.*, 1998; Bachem *et al.*, 1998; Omary *et al.*, 2007). In common with hepatic stellate cells, they are characterized as retinol/lipid-storing cells expressing a variety of intermediate filament proteins including desmin and glial fibrillary acid protein (GFAP) (Wake, 1980; Kordes *et al.*, 2009). Under physiological conditions

This article was published online ahead of print in MBoC in Press (http://www.molbiolcell.org/cgi/doi/10.1091/mbc.E10-10-0807) on December 9, 2010.

Address correspondence to: David I. Yule (David_Yule@urmc.rochester.edu).

Abbreviations used: aPSC, activated pancreatic stellate cells; BrdU, 5-bromo-2′-deoxyuridine; BSA, bovine serum albumin; CCh, carbachol; CCK, cholecystokinin; DIC, differential interference contrast; ECM, extracellular matrix proteins; ER, endoplasmic reticulum; FBS, fetal bovine serum; GBSS, Gey's balanced salt solution; GFAP, glial fibrillary acid protein; IP, intraperitoneal; MAPK, mitogen-activated protein kinase; MP-microscopy, multiphoton microscopy; PAR, protease activated receptors; PBS, phosphate-buffered saline; PDAC, pancreatic ductal adenocarcinomas; PDGF, platelet-derived growth factor; PSC, pancreatic stellate cells; PV, parvalbumin; qPSC, quiescent pancreatic stellate cells; α-SMA, α-smooth muscle actin; WT, wild-type.

© 2011 Won *et al.* This article is distributed by The American Society for Cell Biology under license from the author(s). Two months after publication it is available to the public under an Attribution–Noncommercial–Share Alike 3.0 Unported Creative Commons License (http://creativecommons.org/licenses/by-nc-sa/3.0).

"ASCB®," "The American Society for Cell Biology®," and "Molecular Biology of the Cell®" are registered trademarks of The American Society of Cell Biology.

stellate cells appear to be benign, and relatively little is known regarding their contribution to the normal function of the gland.

PSC have, however, attracted considerable interest because of their prominent role in the etiology of pancreatic pathology (Omary *et al.*, 2007). For example, in disease states of the pancreas including chronic pancreatitis and pancreatic cancer, stellate cells undergo a phenotypic transformation to a so-called activated form. Activated PSC (aPSC) are highly proliferative and adopt a myofibroblastic state characterized by enlargement of the endoplasmic reticulum (ER) and nucleus together with the expression of α-smooth muscle actin (α-SMA). Significantly, aPSC, again similarly to hepatic stellate cells, produce large amounts of extracellular matrix proteins (ECM) resulting in the extensive pancreatic fibrosis observed in disease states (Wake, 1980; Apte *et al.*, 1998, 2004; Haber *et al.*, 1999; Casini *et al.*, 2000; Omary *et al.*, 2007; Kordes *et al.*, 2009).

In vivo, it is likely that the signal transduction pathways that initiate and maintain the activated phenotype are elicited by events triggered by insult and mediated by surrounding cells including infiltrating leukocytes and damaged acinar cells. Much of the current understanding of the stellate cell signal transduction has been gleaned from studies of rodent PSC, isolated and maintained in culture. Initially the cultured cells express markers consistent with a quiescent phenotype, including the presence of prominent cytoplasmic lipid droplets (Apte *et al.*, 1998). However, following short-term culture, cells transform to an activated, proliferative phenotype expressing abundant α-SMA and ECM proteins (Haber *et al.*, 1999). Using this paradigm, inflammatory agents, growth factors, reactive oxygen species, and autocrine/paracrine factors have been shown to act on stellate cells (Omary *et al.*, 2007). For example, aPSC proliferate in response to platelet-derived growth factor (PDGF) and transforming growth factor-β as well as proinflammatory cytokines (Apte *et al.*, 1999; Luttenberger *et al.*, 2000; Shek *et al.*, 2002). These studies have implicated the MAP kinase cascade and JAK/STAT and SMAD pathways as contributing to the processes of transformation and proliferation in PSC (Masamune *et al.*, 2004; Ohnishi *et al.*, 2004; Kikuta *et al.*, 2006). There is, however, a relative lack of data relating to other signaling systems that could potentially result in cell growth and/or transformation. In hepatic stellate cells, intracellular Ca^{2+} signals have been reported to induce proliferation (Soliman *et al.*, 2009). Furthermore, agents proposed to act on PSC, including growth factors and angiotensin II, have the potential to couple to signal transduction pathways, which results in intracellular Ca^{2+} elevations (Luttenberger *et al.*, 2000; Hama *et al.*, 2006). Little information is available regarding the agonists linked to intracellular Ca^{2+} signaling in PSC together with the specific temporal and spatial characteristics of these signals. Moreover, data are lacking relating to the functional consequences of elevations in intracellular Ca^{2+}.

Given this gap in knowledge, the goals of the present study were to characterize Ca^{2+} signaling events and the consequences of these signals in cultured PSC in the quiescent (qPSC) and the transformed activated state. An important consideration is that in culture these events may not be identical to those taking place during disease progression in situ. Therefore, to study these events under conditions where the architecture of the pancreas and structural relationship between cell types are relatively unperturbed, the studies are extended to investigate Ca^{2+} signaling in lobules of intact pancreas using multiphoton (MP) microscopy in both physiological situations and in a model of chronic pancreatitis. Data are presented that provide evidence that the complement of cell surface receptors coupled to Ca^{2+} signaling is altered during activation of PSC, effectively providing a diagnostic feature of the activated phenotype. Further, the specific spatial characteristics of the Ca^{2+} signal are important for enhancing proliferation of aPSC. In total, these data are consistent with Ca^{2+} signaling events triggered by factors, including those likely released following initial acinar cell damage, resulting in proliferation of PSC and contributing to the pathology of disease.

RESULTS

Characterization of Ca^{2+} signaling in cultured qPSC

PSC undergo morphological and phenotypic changes in culture (Apte *et al.*, 1998). To establish the temporal sequence of these changes, PSC morphology and expression of established protein markers were monitored after isolation. On day 2 in culture, cells displayed prominent perinuclear structures, which appeared phase bright (Figure 1Aa) and stained with the lipid marker AdipoRed (Figure 1Ab). The lipid droplets could also be visualized following MP excitation at 810 nm of intrinsic fluorescence, consistent with the presence of vitamin A in the droplets known to fluoresce when excited at this wavelength (Figure 1A, c and d) (Zipfel *et al.*, 2003). Abundant expression of the intermediate filament protein vimentin (Figure 1Ae), together with low levels of desmin and GFAP (unpublished data) were also observed in cells fixed with paraformaldehyde and processed for immunocytochemistry. In contrast, at this time point, the cells did not stain for α-SMA, the prototypical marker for aPSC (Figure 1Af). Intracellular Ca^{2+} signals were also monitored in fura-2–loaded qPSC using digital imaging on day 2 in culture following isolation. An increase in $[Ca^{2+}]_i$ was observed in qPSC in response to a high concentration of the muscarinic agonist carbachol (CCh; >1 μM), typically consisting of oscillatory changes in the $[Ca^{2+}]_i$, even at concentrations as high as 10 μM (Figure 1Ba). qPSC also responded to angiotensin II (>100 nM; Figure 1Bb), bradykinin (>100 nM; Figure 1Bc), and ATP (>1 μM; Figure 1C). The initial Ca^{2+} peak in response to these agonists was largely independent of extracellular Ca^{2+} and thus is likely the result of the $G\alpha_q$-coupled formation of $InsP_3$ and Ca^{2+} release from intracellular compartments (Figure 1D). No elevation in $[Ca^{2+}]_i$ was evoked in qPSC when exposed to 50 mM KCl, trypsin, or thrombin, indicating that qPSC are unlikely to express voltage-gated Ca^{2+} channels or the protease-activated receptors (PAR) family of $G\alpha_q$-coupled cell surface receptors (Figure 1E). In addition, stimulation of qPSC with PDGF or cholecystokinin (CCK) did not result in an elevation of $[Ca^{2+}]_i$ (unpublished data).

Characterization of aPSC in culture

By day 5 in culture, phase-bright lipid droplets were not visible and the cells had adopted a more flattened myofibroblast-type morphology accompanied by the expression of α-SMA in a fraction of cells (Figure 2Aa). All cells expressed α-SMA by day 7 (Figure 2Ab) together with increased expression of vimentin (Figure 2Ac) and desmin (Figure 2Ad). The changes in morphology and expression profile are typical of the transformation of qPSC to the activated phenotype. Ca^{2+} signaling was also studied after day 7 in culture, when all cells express α-SMA and are assumed to represent an activated phenotype. In a similar manner to qPSC, aPSC exhibited an increase in $[Ca^{2+}]_i$ in response to angiotensin II (>100 nM; Figure 2Ba) and bradykinin (>100 nM; Figure 2Bb) but not 50 mM KCl (Figure 2Bc) or CCK up to 50 nM (unpublished data). Exposure of aPSC to ATP also resulted in an increase in $[Ca^{2+}]_i$ (Figure 2C); however, the threshold for eliciting a response was approximately threefold lower in aPSC when compared with qPSC (Figure 2D). In contrast to qPSC, aPSC were refractory to stimulation with CCh at concentrations as high as 10 μM (Figure 2Ea) but elicited robust elevations in Ca^{2+} in response to the PAR agonists thrombin (Figure 2Eb) and trypsin (Figure 2Ec) and to PDGF (Figure 2Ed). In a similar fashion, human stellate cells exhibited morphological markers of aPSC when monitored at day 7 in culture,

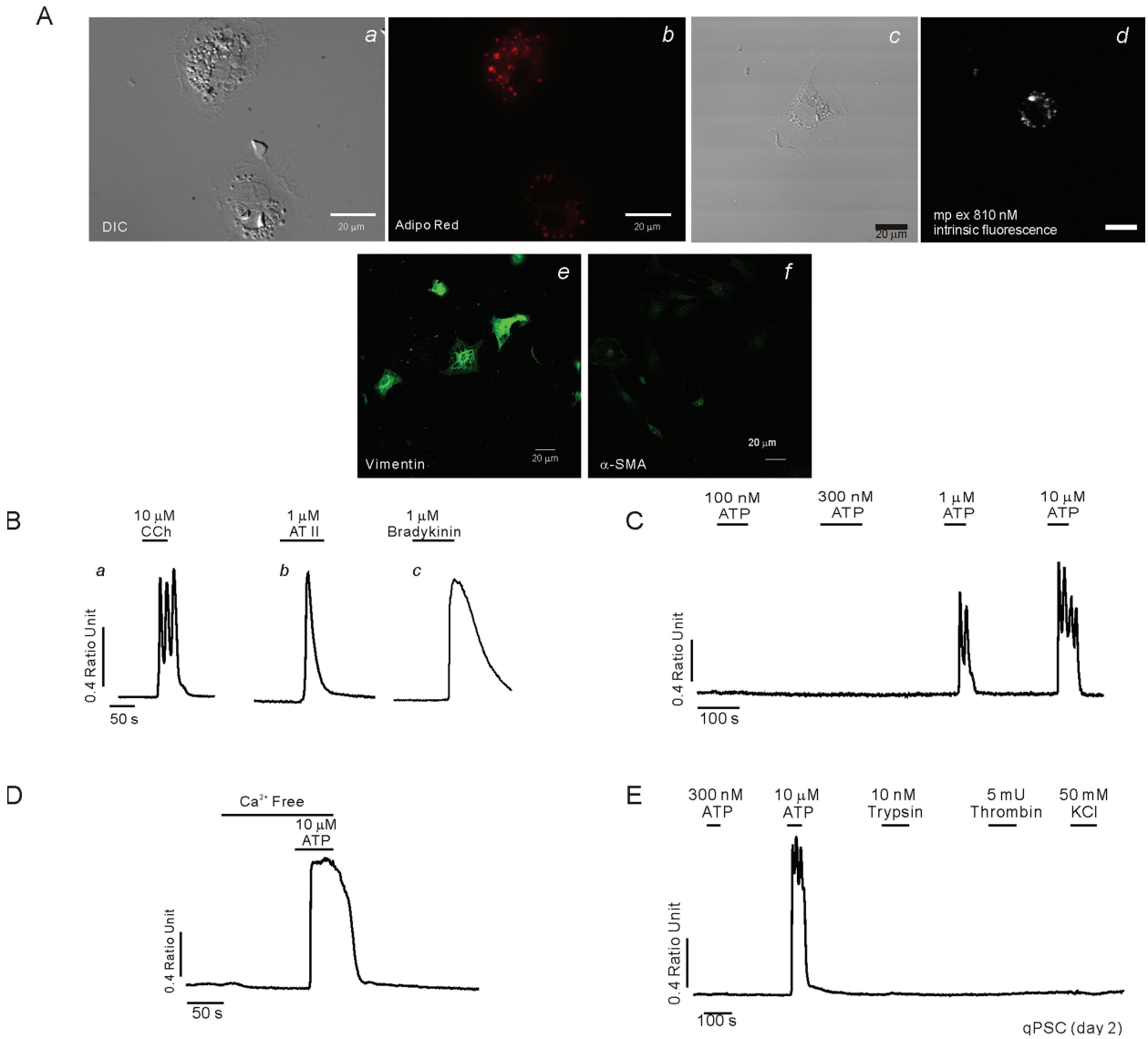

FIGURE 1: Characterization of qPSC in culture. A morphological characterization is shown in (A). (Aa) Typical differential interference contrast (DIC) images of qPSC at day 2 in culture. (Ab) The same cells stained with the lipid marker Adipo Red, indicating prominent perinuclear granules. (Ad) Intrinsic fluorescence with MP excitation at 810 nm, consistent with the presence of vitamin A in the lipid droplets. (Ae) Immunohistochemical staining with vimentin. (Af) Absence of staining with α-SMA. (B–E) Representative Ca^{2+} imaging data from qPSC at day 2 in culture. Cells respond to CCh (Ba), angiotensin (Bb), and bradykinin (Bc) and ATP (C). (D) The initial ATP-induced Ca^{2+} signal is largely independent of extracellular Ca^{2+}. (E) qPSC do not respond to trypsin, thrombin, or membrane depolarization with KCl.

including α-SMA expression, prominent GFAP, and desmin and vimentin staining (Supplemental Figure 1A). These cells responded robustly to PAR-1 and PAR-2 agonists and bradykinin but were also refractory to stimulation with CCK up to 50 nM (Supplemental Figure 1B). The absence of CCK-stimulated Ca^{2+} signals in both mouse and human PSCs is, however, not consistent with two recent studies that have indicated that both CCK-1 and CCK-2 receptors are expressed on human (Phillips *et al.*, 2010) and rat PSC (Berna *et al.*, 2010). It should be noted that neither study monitored CCK-stimulated Ca^{2+} signaling events; thus the formal possibility exists that CCK receptors in PSC do not signal in a conventional manner. The human study suggested that CCK stimulation resulted in acetylcholine release without affecting PSC proliferation or the mitogen-activated protein kinase (MAPK) signaling module. In contrast, the latter study demonstrated robust proliferation in response to CCK that was mediated by the MAPK and phosphatidylinositol 3-kinase signaling cascades. Although the reasons for these discrepancies are not clear, it is possible that species differences or variations in the phenotypic state of the PSC examined might contribute to this lack of accord.

Periacinar cells in pancreatic lobules have characteristics of qPSC

To evaluate the phenotype of PSC in situ in terms of Ca^{2+} signaling characteristics, pancreatic lobules were prepared from wild-type (WT) animals and loaded with both Fluo-4 AM and calcein AM. The latter dye was used to visualize lobule structure independently of $[Ca^{2+}]_i$. Figure 3 shows a maximum projection image of a lobule (~120 µm thick) generated using MP microscopy of calcein fluorescence at the indicated magnifications (Figure 3A). Because the lobules were prepared without enzymatic digestion and with minimal preparative

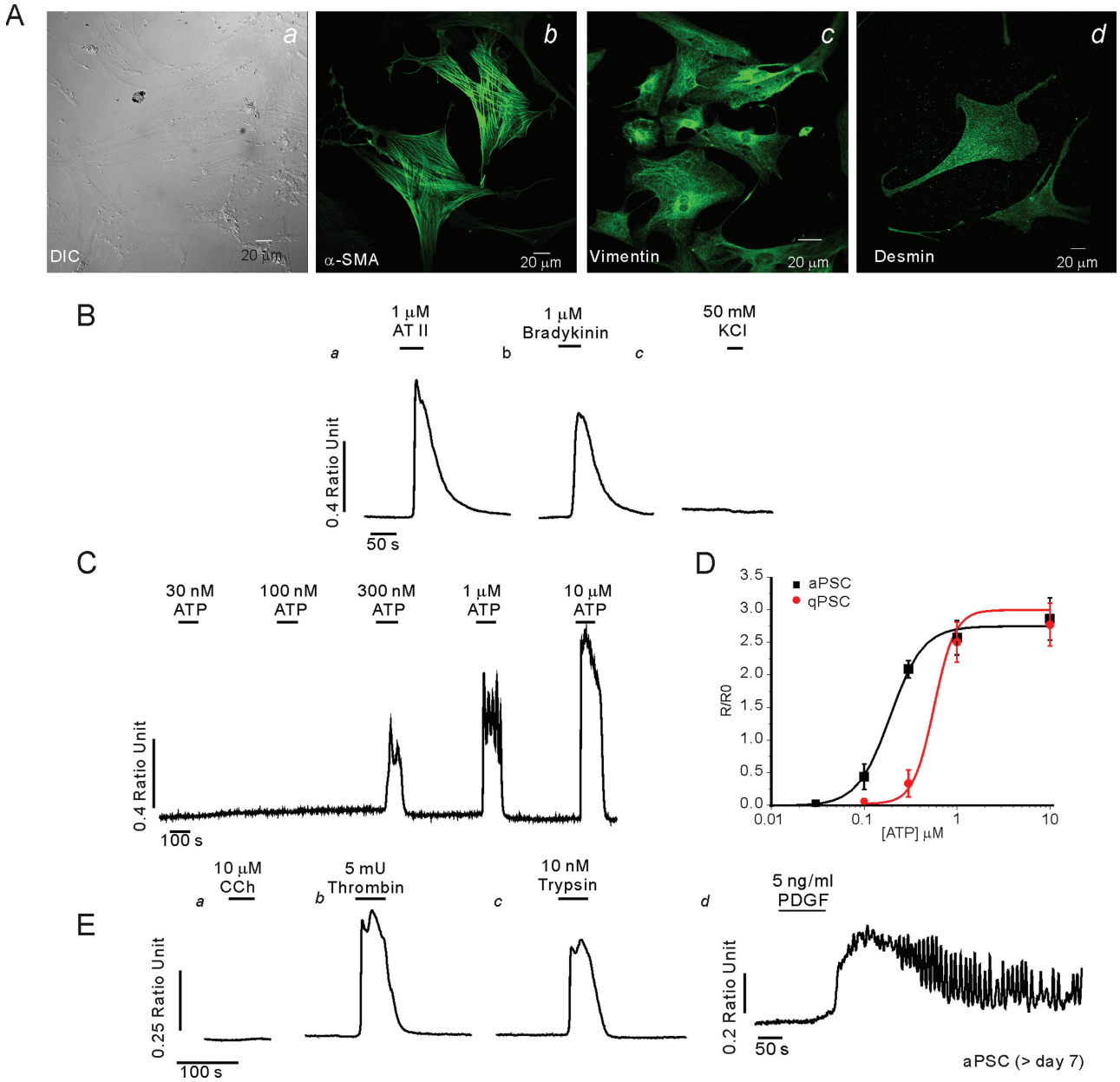

FIGURE 2: Characterization of aPSC in culture. A morphological characterization is shown in (A). (Aa) Typical DIC images of aPSC at day 7 in culture. Prominent staining with α-SMA (Ab), vimentin (Ac), and desmin (Ad). (B–E) Representative Ca^{2+} imaging data from aPSC at day 7 in culture. Increases in $[Ca^{2+}]_i$ were evoked by angiotensin (Ba) and bradykinin (Bb) but not KCl (Bc). (C) Cells responded to ATP. (D) Comparison of the concentration vs. response relationship for the ATP-evoked change in peak height in aPSC vs. qPSC. In contrast to qPSC, aPSC did not increase Ca^{2+} when challenged with CCh (Ea), but thrombin (Eb), trypsin (Ec), and PDGF (Ed) evoked robust elevations in $[Ca^{2+}]_i$.

intervention, the tissue retained obvious exocrine morphology, exemplified by the phase-dark apical localization of zymogen granules in the acinar clusters. In identical lobules prepared for immunocytochemistry, acinar cells could be readily visualized by the expression of α-amylase while vimentin was distributed in periacinar/ductal cells (Figure 3B). α-SMA was expressed only in ductal structures, indicating the scarcity/absence of aPSC in this preparation. Nonacinar cells could also be readily visualized in the live lobules, including cells with a periacinar distribution, which exhibited preferential loading of both fluorescent dyes (Figure 3A, arrows). Periacinar cells also exhibited prominent punctate intrinsic fluorescence when excited at 810 nm, again consistent with the presence of vitamin A in lipid droplets of qPSC (Figure 3A). The morphology of these cells could also be clearly distinguished from neurons visualized in pancreatic lobules isolated from animals engineered to express green fluorescent protein specifically in neurons. These cells were relatively rare in the fields selected and characterized by long projections extending from the cell bodies (Supplemental Figure 2). In this population of periacinar cells, robust $[Ca^{2+}]_i$ changes could be evoked by ATP (>1 μM) (Figures 4, A, images, and B–F, kinetics) as well as bradykinin (Figure 4C), angiotensin (Figure 4D), and high concentrations of CCh (Figure 4E). An increase in $[Ca^{2+}]_i$ was never observed in periacinar cells in lobules exposed to thrombin (Figure 4E), trypsin (Figure 4F), CCK (Figure 4C), or PDGF (unpublished data). However, acinar cells in the

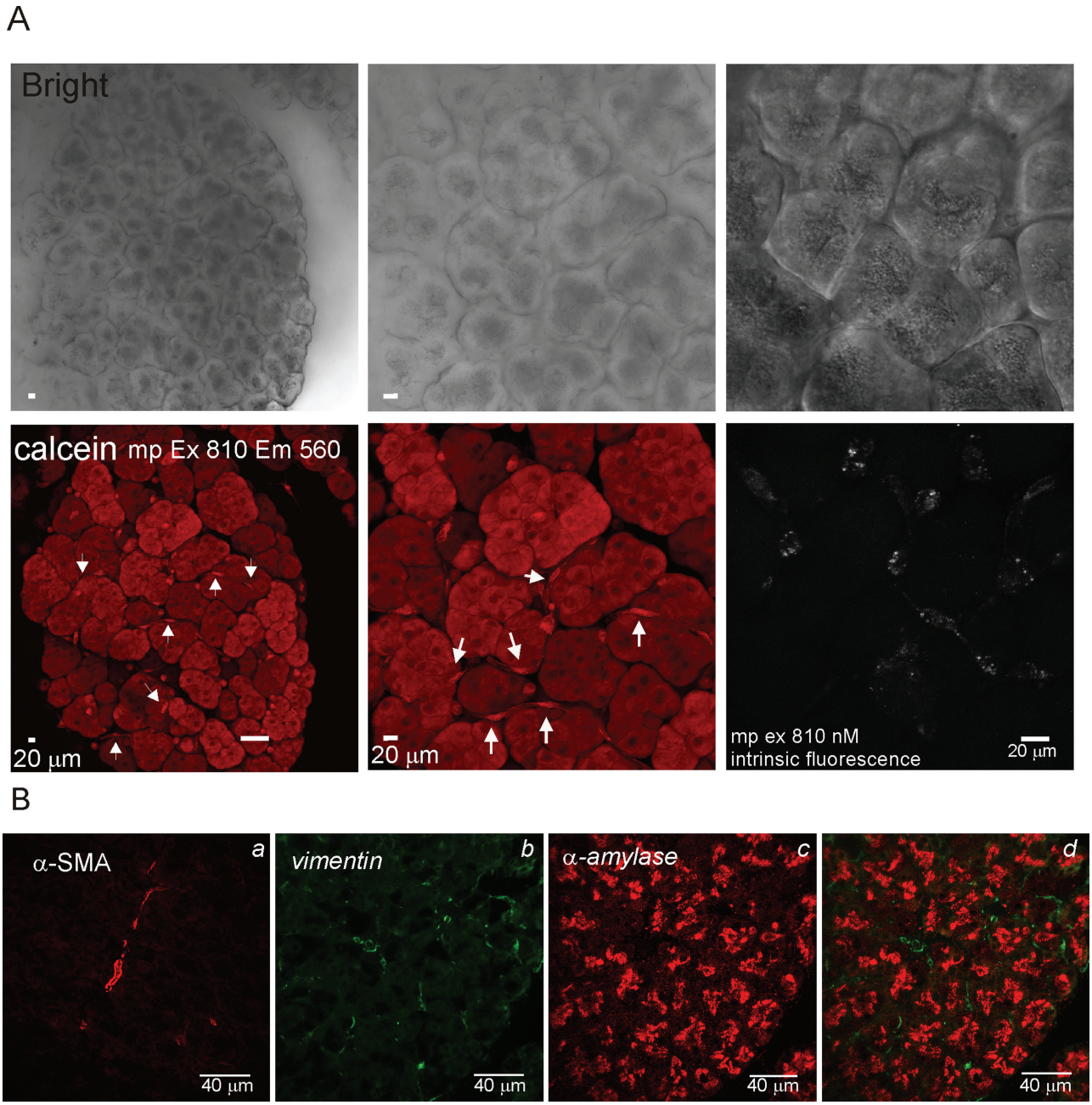

FIGURE 3: Characterization of pancreatic lobules. (A, top) Transmitted laser light images of a pancreatic lobule at magnification of 25× (left) and 50× (middle). The left panel shows intrinsic fluorescence in periacinar cells with MP excitation at 810 nm. (A, bottom) Corresponding MP-excitation images of calcein fluorescence. Arrows indicate nonacinar cells. (B) Immunocytochemical staining of fixed pancreatic lobules. Prominent duct cell staining of α-SMA (Ba), periacinar staining for vimentin (Bb), and acinar staining with α-amylase (Bc); overlay of Bb/Bc is shown in Bd.

same fields could be clearly shown to increase $[Ca^{2+}]_i$ in response to CCK (Figure 4C, red trace), trypsin (Figure 4F, red trace), and CCh (unpublished data). Together, these data demonstrate the utility of measuring Ca^{2+} signals in situ in pancreatic lobules and importantly show that periacinar-localized cells from WT animals have Ca^{2+} signaling characteristics consistent with those of qPSC in culture.

Characterization of PAR agonist–induced $[Ca^{2+}]_i$ signals in aPSC

Because of the probable pathophysiological significance of protease-activated signaling in pancreas (Namkung *et al.*, 2004; Masamune *et al.*, 2005; Laukkarinen *et al.*, 2008), experiments were performed to define in detail the characteristics of PAR-induced $[Ca^{2+}]_i$ in aPSC. PAR are activated as proteases attack a cleavage site toward the N-termini of the receptor, revealing a previously cryptic tethered peptide ligand (Soh *et al.*, 2010). Synthetic peptides consisting of six amino acids upstream of the cleavage site can activate the receptor independently of protease cleavage. The PAR family is encoded by four genes, and although the selectivity is not exclusive, thrombin preferentially cleaves PAR-1 and -3 whereas trypsin has been shown to act on PAR-2 and -4. Activated PAR can couple to multiple heterotrimeric G protein α-subunits including $G_{\alpha 1}$, $G_{\alpha 12/13}$, and $G_{\alpha q/11}$. Thus direct activation of PLC by $G_{\alpha q}$ or $G_{\beta\gamma}$ subunits are linked to Ca^{2+} signaling events. Proteases may activate

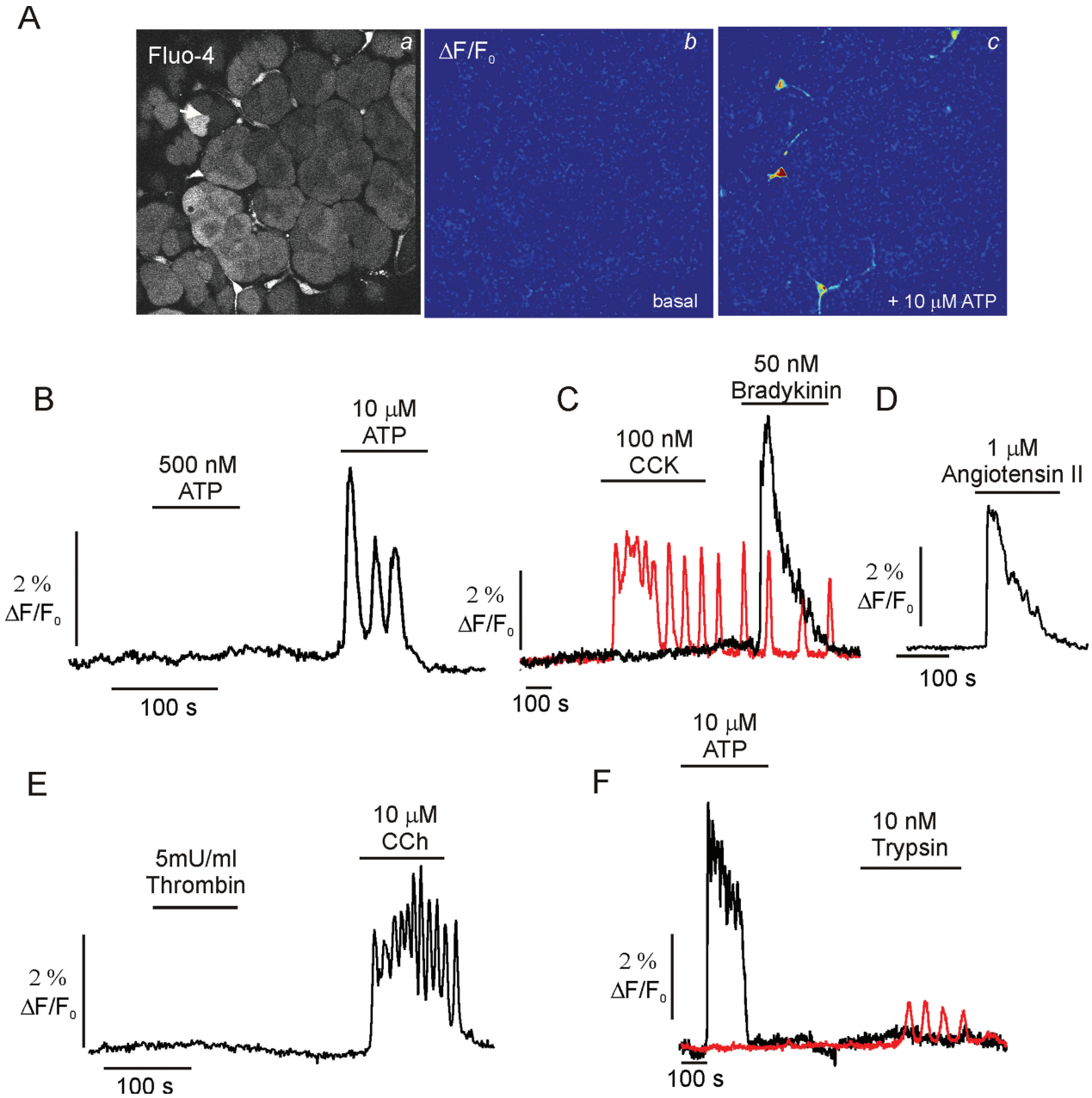

FIGURE 4: MP imaging of Ca^{2+} signals in pancreatic lobules. (A) A typical MP-imaging experiment is shown. (Aa) MP image of a lobule loaded with Fluo-4 AM. (A, b and c) $\Delta F/F_0$ images before and after ATP exposure, respectively. (B) Representative $[Ca^{2+}]_i$ trace from a periacinar cell responding to ATP exposure. (C) A periacinar cell responds to bradykinin but not CCK (black trace) while an acinar cell in the same field responds to CCK (red trace). (D) Typical response to angiotensin. (E) A periacinar cell responds to CCh but not thrombin. (F) An acinar cell (red trace) but not a periacinar cell responds to trypsin exposure.

multiple PAR subtypes, and therefore synthetic peptides modeled on the sequence of the ligand were next used to define the PAR subtypes expressed in aPSC. A marked elevation in $[Ca^{2+}]_i$ was evoked by the PAR-1 receptor peptide ligand (Figure 5, Aa and B) with an apparent K_d of ~300 nM. Increasing PAR-1 peptide resulted in a recruitment of responsive aPSC; above 300 nM peptide > 80% of cells responded (Figure 5C), and a corresponding decrease in latency between ligand exposure and the elevation in $[Ca^{2+}]_i$ was observed (Figure 5D). The PAR-2 ligand evoked a smaller increase in $[Ca^{2+}]_i$ and was less potent (Figure 5Ab). In contrast, ligands directed against PAR-3 and PAR-4 were without effect (Figure 5, Ac and Ad, respectively).

During the previous series of experiments, it was noted that PAR ligands, ATP, and PDGF-stimulated Ca^{2+} elevations were not spatially homogeneous. The spatial characteristics of the Ca^{2+} signal were therefore next studied in Fluo-4–loaded aPSC. Following exposure to PAR-1 ligand (Figure 6, A and B), PDGF (Figure 6, C and D), or ATP (Figure 6, E and F), the Ca^{2+} signal was initiated close to the nucleus and propagated freely into the nucleus and surrounding cytoplasm. The fluorescence signal was invariably greater within the nucleus when compared with the cytoplasm and margins of the cell (Figure 6). Ca^{2+}-sensitive dyes have been reported to behave anomalously in the nuclear milieu and often overestimate the magnitude of signals (Bootman *et al.*, 2009). Nevertheless, these data show that

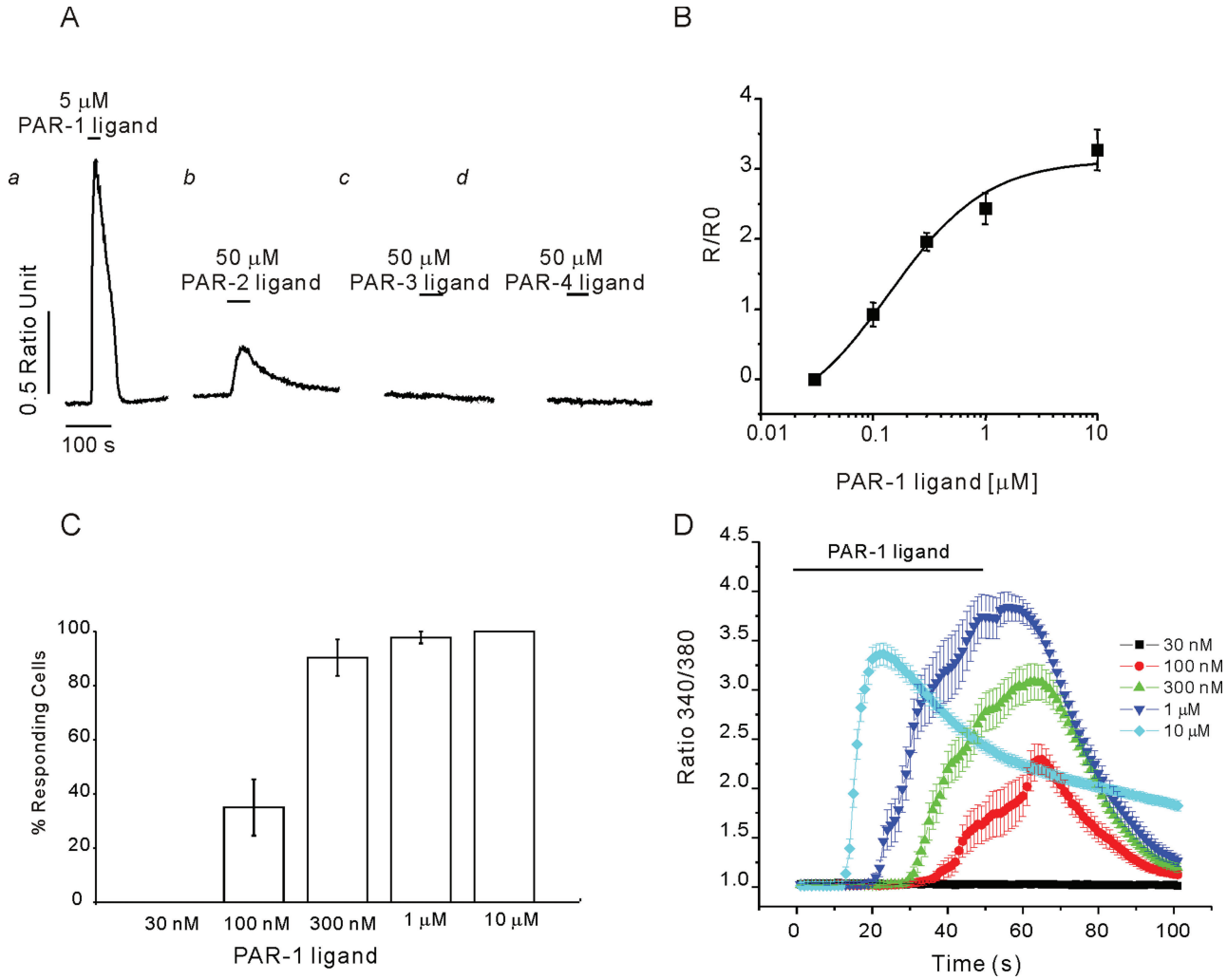

FIGURE 5: Characterization of PAR Ca^{2+} signaling in aPSC in culture. (A) Ca^{2+} elevations could be evoked in aPSC following exposure to peptide PAR-1 peptide ligand (SFLLRN-NH_2) (Aa) and PAR-2 peptide ligand (SLIGRL-NH_2) (Ab) but not PAR-3 (SFNNGGP-NH_2) (Ac) or PAR-4 ligand (AYPGKF-NH_2) (Ad). (B) Concentration vs. response relationship for the peak Ca^{2+} response evoked by PAR-1 ligand. (C) Increasing PAR-1 ligand results in progressive recruitment of cells to increase Ca^{2+} (increase defined as > 0.02 ratio units change from basal). (D) Mean data showing the change in latency and peak height of the Ca^{2+} signal initiated by increasing [PAR-1] ligand.

Ca^{2+} appears to be readily released or diffuses from local release sites to maintain an elevated [Ca^{2+}] in the nucleoplasm of aPSC.

The spatial organization of the Ca^{2+} signals was further investigated using focal production of $InsP_3$ in distinct, spatially separated regions of aPSC (~1.5 μm^3 focal volume) using laser photolysis of a cell-permeable form of caged $InsP_3$ (ci-$InsP_3$) (Won *et al.*, 2007). When the laser light was focused in the nucleus, low levels of photolysis resulted in elevated fluorescence signals that were largely confined to this compartment (Figure 7A, small arrow). Increasing energy produced larger nuclear signals that were maintained over an extended time period (>20 s). The signals also propagated into the surrounding cytoplasmic regions (Figure 7, A, large arrow; B, images). Positioning the laser spot in the margins of the cell ~20 μm distant from the nucleus resulted in an initial increase in Ca^{2+} signal at the photolysis site followed by a robust, maintained signal in the nucleus (Figure 7, C and D). Together, these data again support the idea that in aPSC, Ca^{2+} signals are freely communicated into the nuclear compartment and are consistent with $InsP_3$-induced Ca^{2+} release occurring either in, or directly surrounding, the nucleus.

Nuclear Ca^{2+} signals stimulate proliferation of aPSC

To investigate further the mechanism underlying the compartmentalized Ca^{2+} signals and to probe their physiological role, we utilized a series of adenoviruses expressing Ca^{2+} buffers targeted to specific cellular compartments (Rodrigues *et al.*, 2007). The constructs consist of parvalbumin (PV) linked to the red fluorescent protein DsRed, and either a nuclear localization sequence (PV-NLS-DsRed) or nuclear exclusion signal (PV-NES-DsRed). Figure 8Aa shows a cell expressing a nontargeted PV-DsRed construct following virus infection and demonstrates the heterogeneous expression of the chimeric protein in aPSC. In contrast, PV-NES-DsRed was expressed in the cytoplasm and excluded totally from the nucleus (Figure 8Ab) while PV-NLS-DsRed was exclusively expressed only in the nucleus of aPSC (Figure 8Ac). Essentially 100% of cells were infected with each adenovirus, as evidenced by the presence of uniform red fluorescence. The impact on the Ca^{2+} signal of compartmentalized PV expression was assessed in Fluo-4–loaded aPSC stimulated with PAR-1 ligand. Expression of nontargeted PV resulted in a marked dampening of the agonist-evoked Ca^{2+} signals throughout the cell when

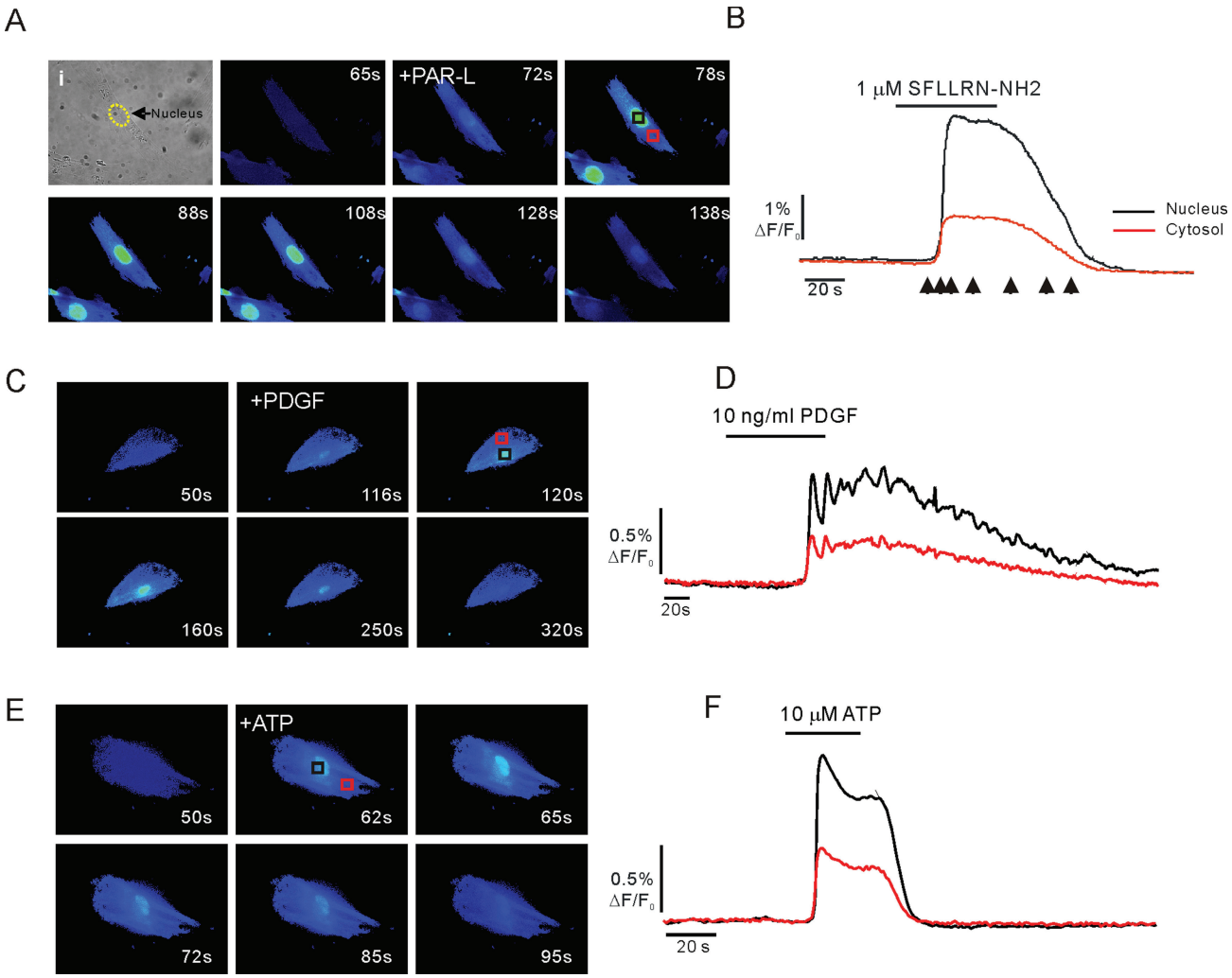

FIGURE 6: Spatial characteristics of Ca^{2+} changes. Exposure to PAR agonist evokes prominent, sustained fluorescence changes in the nucleus of aPSC (A, black trace) vs. a cytoplasmic region of interest (A, red trace). (B) Corresponding images acquired at time points corresponding to the arrows in (A). (C, images; D, kinetics) PDGF stimulation results in similar prominent nuclear Ca^{2+} signals. (E, images; F, kinetics) ATP stimulation results in prominent nuclear Ca^{2+} signals.

compared with non-PV construct–expressing cells (Figure 8Ba). In cells expressing PV-NES-DsRed, the Ca^{2+} signal in the extranuclear region was largely abolished (Figure 8Bb). However, a robust nuclear Ca^{2+} signal was still observed. Conversely, expression of PV-NLS-DsRed resulted in a markedly dampened nuclear Ca^{2+} signal, although the cytoplasmic signal was largely preserved (Figure 8Bc), indicating, not unexpectedly, that Ca^{2+} release can occur at some distance away from the nucleus.

aPSC are highly proliferative, and expansion of cell numbers followed by secretion of ECM is thought to play a major role in disease progression in chronic pancreatitis. Experiments were subsequently performed using targeted buffers to evaluate whether the prominent compartmentalized increases in $[Ca^{2+}]_i$ play any role in promoting cell proliferation. aPSC were serum deprived for 16 h before addition of media replete with 1% fetal bovine serum (FBS). Proliferation was assessed by monitoring incorporation of 5-bromo-2′-deoxyuridine (BrdU) 24 h later. Addition of FBS resulted in a significant increase in BrdU incorporation. Basal proliferation in the absence of FBS was unaffected regardless of the expression and localization of targeted PV, while incorporation of BrdU was significantly increased in cells not expressing PV constructs exposed to FBS (Figure 9). Global uniform expression of PV (PV-DsRed) or buffering of cytoplasmic Ca^{2+} specifically with PV-NES-DsRed did not alter the proliferation of aPSC. In contrast, expression of PV-NLS-DsRed and thus buffering of nuclear Ca^{2+} completely eliminated proliferation (Figure 9). These data highlight the general importance of nuclear Ca^{2+} changes for proliferation and strongly suggest that agents that increase nuclear $[Ca^{2+}]$, including PAR agonists, PDGF, and ATP, likely present in or around the gland following insult and play an important role in aPSC proliferation.

PSC in an animal model of chronic experimental pancreatitis

LSL-K-Ras^{G12D} mice express an activating mutation of the oncogene K-Ras driven by its endogenous promoter in acinar cells and thus exhibit moderately elevated Ras activity in acinar cells (Ji *et al.*, 2002; Guerra *et al.*, 2007). The animals develop extensive pancreatic fibrosis only following induction of experimental pancreatitis with serial intraperitoneal (IP) cerulein injections. These mice therefore provide an excellent model system to study Ca^{2+} signaling in PSC during the development of fibrosis. Studies were performed in lobules prepared from LSL-K-Ras^{G12D} mice under control conditions and subsequently following cerulein injection as detailed in *Materials*

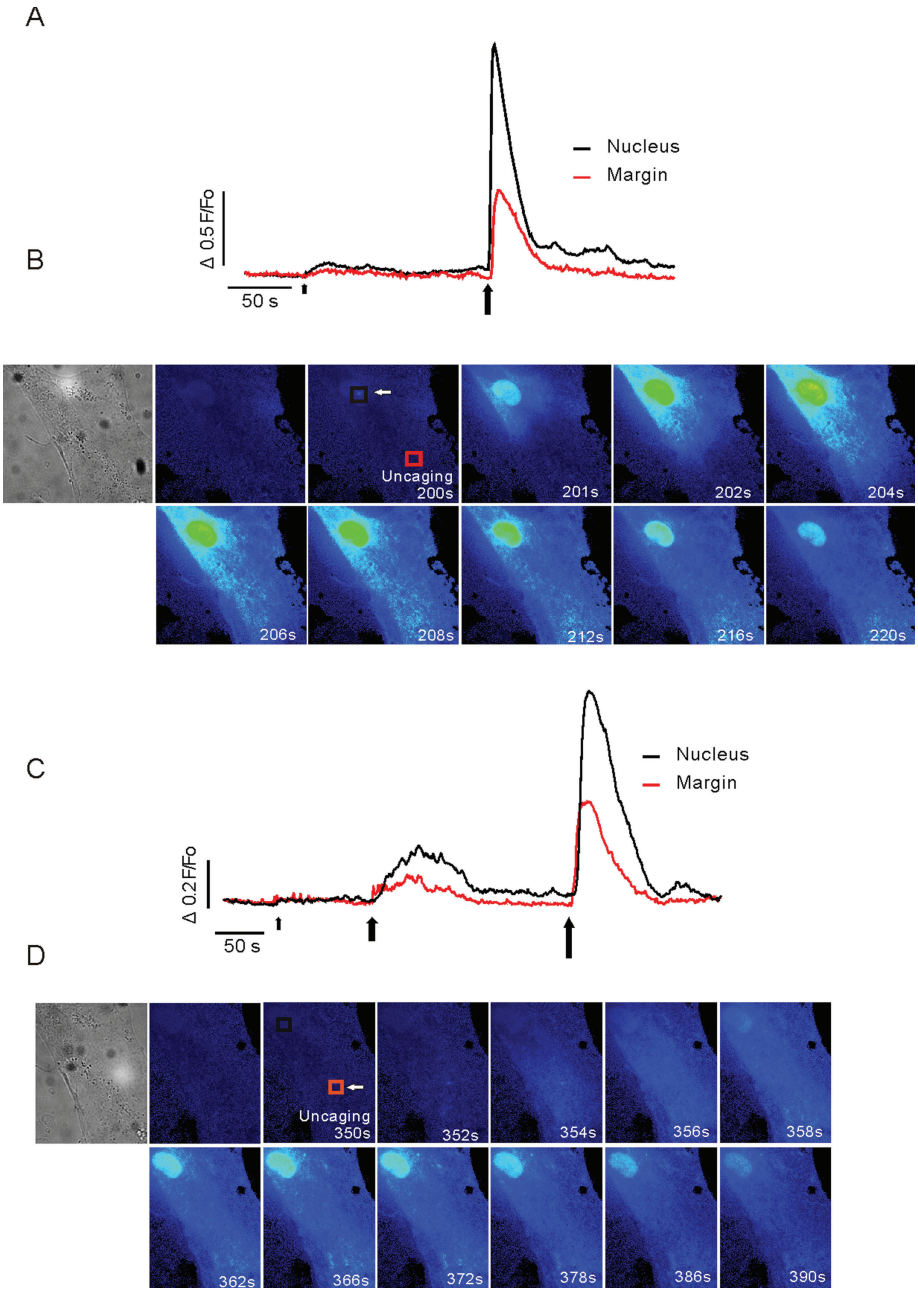

FIGURE 7: Spatial characteristics of Ca^{2+} signals in aPSC following focal uncaging of ci-$InsP_3$. (A and B) Response to focal production of ci-$InsP_3$ in a ~1.5-μm^3 region located close to the nucleus. The kinetic trace showing a region of interest located ~20 μm from the uncaging site (red trace) or in the nucleus (black trace). The arrowheads indicate the time/duration of uncaging (small arrow, 25 ms; larger arrow, 50 ms exposure to laser light). The images in (B) correspond to the indicated times following the second uncaging. Prominent, sustained changes in fluorescence are observed in the nucleus. (C and D) ci-$InsP_3$ is produced some 20 μm from the nucleus (small arrow, 25 ms; large arrow, 50 ms; largest arrow, 75 ms). Kinetic and corresponding images following the final uncaging are shown in (C) and (D), respectively. A robust change in fluorescence is evoked and maintained in the nucleus.

and Methods. The morphology of lobules isolated from LSL-K-Ras^{G12D} mice was not dramatically altered from WT animals under these control conditions (Figure 10A). Obvious acinar structures could be readily identified, and the distribution and number of periacinar cells were not significantly altered. However, the morphology of some nonacinar cells appeared enlarged and more flattened than typical of WT cells (arrowhead in Figure 10A; compare with Figure 3). Periacinar cells responded to angiotensin II (Figure 10E), and a proportion of these cells also increased [Ca^{2+}] when exposed to thrombin (Figure 10B; pooled data in Figure 12G) or trypsin (Figure 10C; pooled data in Figure 12H) and low concentrations of ATP (Figure 10D; pooled data in Figure 12I), suggesting that some cells exhibit the phenotype of aPSC. Consistent with this idea, in a limited number of experiments cells also responded to PDGF. Furthermore, when stellate cells were isolated from these animals, α-SMA staining could be observed in 21% of cells on day 2 in culture (Figure 10F, 24/114 cells; 17 fields prepared from two mice), which was much earlier than cells prepared from WT animals (Figure 2), indicating the presence of aPSC in the pancreata of LSL-K-Ras^{G12D} mice (Figure 10F).

Pancreatic lobules from WT and LSL-K-Ras^{G12D} animals were isolated 3 d after induction of experimental pancreatitis as detailed in *Materials and Methods* following IP injection of the CCK analogue cerulein. The structure of lobules from WT animals injected with cerulein was again not markedly different from noninjected WT animals, with sparse localization of α-SMA confined to ductal structures (Supplemental Figure 3). Patent acinar structure and occasional periacinar cells were clearly visualized by MP imaging of calcein fluorescence (Figure 11A, top). In ~50% of these lobules, cells responded to thrombin (9/20 lobules examined) and trypsin (7/13) (Figure 12, A and B; pooled data in Figure 12, G and H), indicative of the presence of aPSC following treatment. This number was similar to noninjected LSL-K-Ras^{G12D} lobules. Similar morphology and lack of proliferation of nonacinar cells were also seen in animals in which the injection protocol was repeated and the animals killed at day 28 (Figure 11C). In contrast, identical treatment of LSL-K-Ras^{G12D} resulted in a severe disruption of exocrine pancreatic structure, a striking increase in the expression of α-SMA (Supplemental Figure 3), and a marked increase in nonacinar cells, presumably PSC (Figure 11, A, bottom, and C). Specifically, in numerous foci there was a loss of acinar cell structure, with the polarized cells replaced by cells with cuboidal morphology (Figure 11A, bottom). Foci were surrounded by numerous elongated cells that preferentially loaded with calcein AM. Paraformaldehyde-fixed lobules from these animals showed extensive expression of α-SMA in rings of cells surrounding cells expressing amylase (Figure 11B). The cells surrounding the remnants of acinar cells are therefore likely aPSC. Consistent with this hypothesis, in ~95% of these lobules, cells were present that increased [Ca^{2+}]$_i$ in response to trypsin, thrombin, and low concentrations of ATP (Figure 12, D–F; pooled data in Figure 12, G–I). This loss

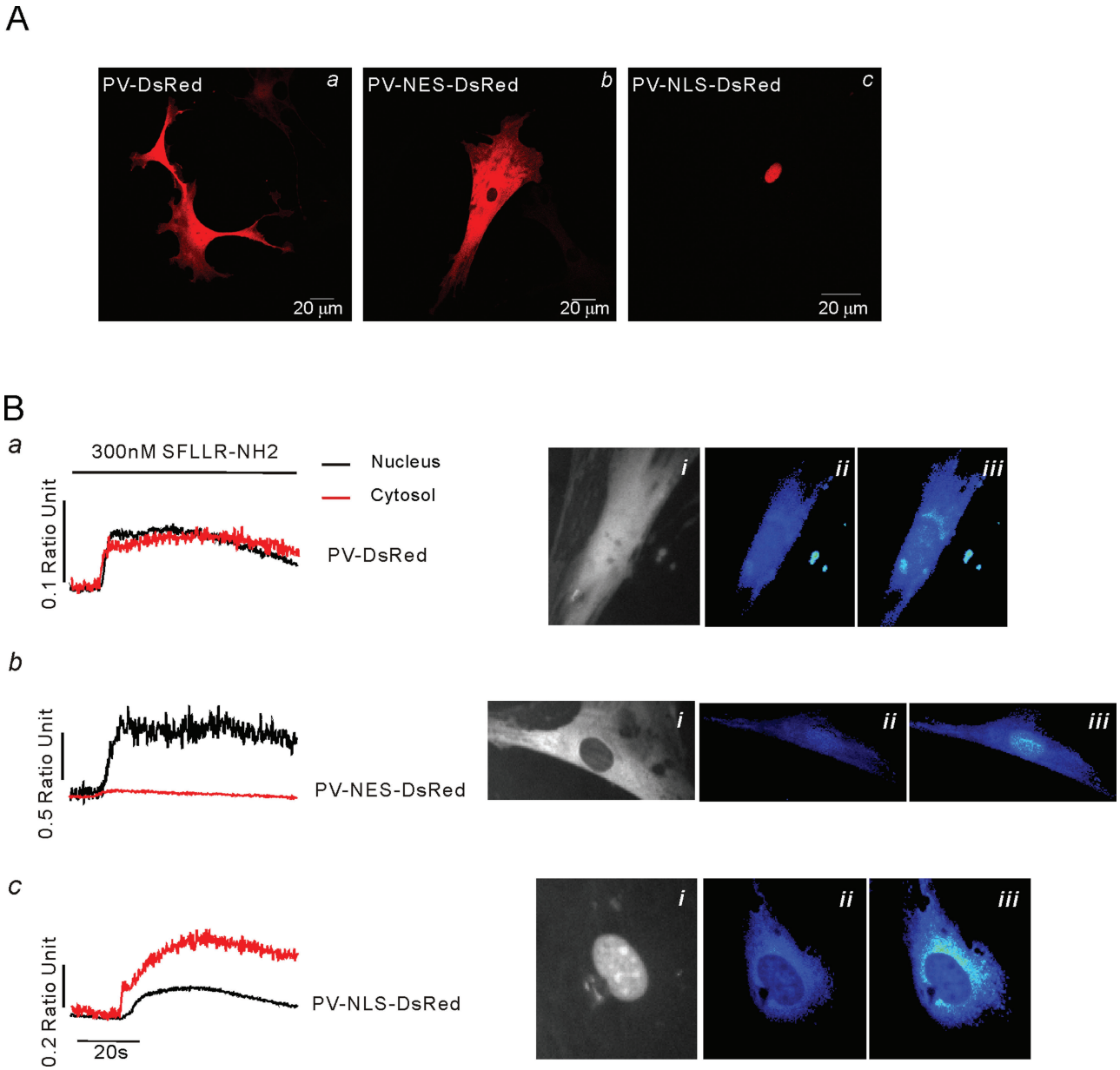

FIGURE 8: Expression of compartment-specific PV constructs. (A) Localization of PV-DsRed (Aa), PV-NES-DsRed (Ab), and PV-NLS-DsRed (Ac) constructs following infection of aPSC with corresponding adenovirus. (B) Representative Ca^{2+} changes in aPSC infected with the indicated construct. (Ba) PV-DsRed dampens $Ca^{2}+$ changes in both nucleus (black trace) and cytoplasm (red trace). (Bai) Localization of construct. (Baii) $\Delta F/F_0$ Fluo-4 image before and (Baiii) after exposure to PAR-1 peptide ligand. (Bb) PV-NES-DsRed dampens Ca^{2+} changes in the cytoplasm (red trace) but not the nucleus (black trace). (Bbi) Localization of PV-NES-DsRed. (Bbii) $\Delta F/F_0$ Fluo-4 image before and (Bbiii) after exposure to PAR-1 peptide ligand. (Bc) PV-NLS-DsRed dampens $Ca^{2}+$ changes in the nucleus (black trace) but not the cytoplasm (red trace). (Bci) Localization of PV-NLS-DsRed. (Bbii) $\Delta F/F_0$ Fluo-4 image before and (Bbiii) after exposure to PAR-1 peptide ligand.

of acinar structure and increase in PSC numbers, as monitored by calcein fluorescence in cells surrounding the foci, were even more marked after 28 d (Figure 11C). However, lobules prepared from these animals loaded very poorly with Fluo-4, precluding extensive investigation of Ca^{2+} signaling events.

DISCUSSION

The central role of Ca^{2+} signaling in pancreatic acinar cells in both health and disease is firmly established (Sutton *et al.*, 2003; Kiselyov *et al.*, 2006; Williams and Yule, 2006; Petersen and Tepikin, 2008). There are, however, relatively few reports characterizing the dynamics and impact of these potentially important signaling events in other exocrine pancreatic cell types. In this study, we have characterized Ca^{2+} signaling events in PSC both in culture and in situ, in acutely isolated lobules. The lobule preparation retains gland architecture that is largely comparable to the native pancreas and therefore provides an excellent platform to study signaling events in the various cell types resident in the exocrine pancreas. Significantly, we demonstrate that the phenotypic changes observed in PSC during activation in culture are mirrored by changes that occur in PSC in situ in WT animals and in an animal model of chronic pancreatitis. In both qPSC and aPSC, Ca^{2+} signaling is initiated via the canonical pathway,

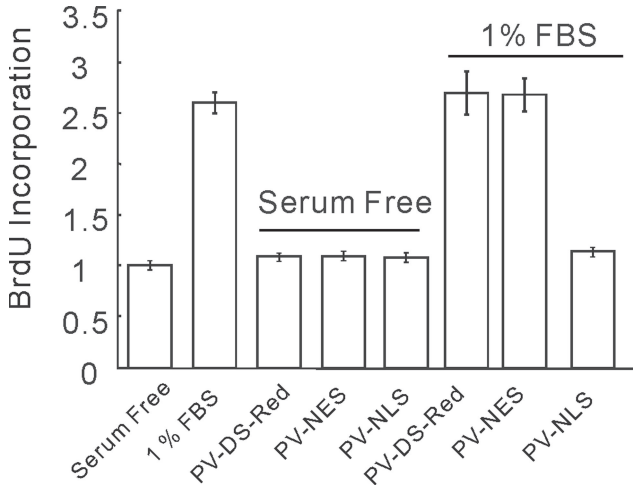

FIGURE 9: aPSC proliferation is attenuated by nuclear-targeted PV. Proliferation induced by serum was attenuated only by PV-NLS-DsRed.

which results in $InsP_3R$-mediated Ca^{2+} release from intracellular stores. Notably, however, the complement of PSC cell–surface receptors coupled to Ca^{2+} signaling events was dramatically altered during activation, and these changes are paralleled whether in culture or in situ. Although the "route" of activation may be different in the case of the animal model versus cultures of acutely isolated PSC, the observation that aPSC in each situation share fundamental similarities provides important validation for studies of cultured PSC.

Ca^{2+} signaling events in cultured aPSC

Agonist-stimulated Ca^{2+} changes are ubiquitous signals controlling a diverse array of downstream effectors that ultimately direct various cellular endpoints as disparate as proliferation and apoptotic cell death (Berridge *et al.*, 2000). It is clear that cells must use mechanisms to ensure fidelity and specificity in order to guarantee the appropriate activation of effectors. This is widely believed to occur as a consequence of the specific temporal and spatial characteristics of the Ca^{2+} change. Stimulation of aPSC in culture resulted in Ca^{2+} signals with distinct spatial features. The signals appear to initiate close to the nuclear envelope, subsequently rapidly invade, and are maintained in the nucleoplasm relative to the cytoplasm. Ca^{2+} signals with similar spatial characteristics were also initiated following focal liberation of $InsP_3$ from a caged precursor some 20 μm distant from the nucleus, suggesting that the generation of nucleoplasmic signals is favored in aPSC. In addition, uncaging directly in the nucleus produced signals that were again maintained in this compartment longer than the corresponding cytoplasmic signals. A question arises as to the mechanism that underlies the striking spatial attributes of the signal. A simple hypothesis is that $InsP_3$ is produced at the plasma membrane, diffuses through the cytoplasm, and engages $InsP_3R$ on perinuclear ER to initiate Ca^{2+} release (Allbritton *et al.*, 1994; Lipp *et al.*, 1997; Eder and Bading, 2007; Bootman *et al.*, 2009). The nucleoplasmic Ca^{2+} rise then passively follows the Ca^{2+} rise from the ER by diffusion through the nuclear pore complex. The signal remains elevated because of the relatively low buffering capacity and paucity of Ca^{2+} ATPase activity within the nucleus (Fox *et al.*, 1997).

Studies using targeted PV indicate, however, that simple diffusion between compartments may not be the complete story. Nuclear but not cytoplasmic Ca^{2+} elevations were markedly attenuated in cells expressing nuclear-targeted PV, indicating, not unexpectedly, that Ca^{2+} signals can be initiated away from the nucleus and are consistent with a contribution of passive diffusion into the nucleus. To the contrary, nuclear Ca^{2+} signals were readily observed in the presence of PV targeted to the cytoplasm where Ca^{2+} was shown to be effectively buffered. This observation is consistent with the notion that the Ca^{2+} signal observed in the nucleoplasm can result from Ca^{2+} release through $InsP_3R$ localized in the close vicinity of the nucleus. Potential release sites with precedent established in other cell types include $InsP_3R$ localized to the outer nuclear envelope, localized to the inner nuclear membrane, or alternatively directly from ER invaginations projecting within the nucleus (Hennager *et al.*, 1995; Echevarria *et al.*, 2003; Cardenas *et al.*, 2010).

Do these nuclear Ca^{2+} changes play any specific role in cultured aPSC? Nucleoplasmic Ca^{2+} changes have been shown to alter the activity of numerous downstream targets including transcription factors, kinases, and phosphatases (Dolmetsch *et al.*, 2001; Pusl *et al.*, 2002; Mellstrom *et al.*, 2008). An elegant demonstration of the profound impact of nuclear Ca^{2+} on cellular function has been reported in a series of studies using targeted PV constructs developed by Nathanson, Leite, and colleagues (Rodrigues *et al.*, 2007). A major finding of these studies was that PV targeted to the nucleus markedly reduced cell proliferation in hepatocytes and the size of hepatic tumors (Rodrigues *et al.*, 2007). The predominant effect of nuclear PV was to block progression through the cell cycle by controlling mitosis. Significantly, cytosolic-targeted PV did not alter cell proliferation but attenuated the activity of cytosolic effectors. The current data indicate that nuclear Ca^{2+} plays an analogous role in aPSC because in a similar fashion simple global attenuation of the Ca^{2+} signal, or specific cytosolic reduction, did not alter proliferation while nuclear-targeted PV selectively abrogated aPSC proliferation. That the specific expression of PV in the nucleus reduced proliferation while a general reduction of $[Ca^{2+}]$ with the nontargeted PV did not, may be related to the fact the NLS construct, as a function of specific targeting and presumably increased relative "residence" in the nucleus, is better able to tightly control the local Ca^{2+} environment in this compartment. Interestingly, these data are in contrast to a report on hepatic stellate cells that indicated that while Ca^{2+} changes were important for proliferation, the specific compartment was not (Soliman *et al.*, 2009). In total, the experiments point to an important role of compartmentalized nuclear Ca^{2+} signals in the proliferation of aPSC. This may contribute to the mechanism's underpinning expansion of aPSC cell numbers in disease states of the pancreas.

Phenotypic changes in cultured PSC on activation: implications for pancreatic disease

A major change during PSC transformation to an activated phenotype is the expression of PAR-1 and PAR-2 receptors (Masamune *et al.*, 2005) and increased sensitivity to ATP. The demonstration of Ca^{2+} signaling events generated following thrombin and trypsin exposure exclusively in aPSC is consistent with these proteins initiating Ca^{2+} signaling events that contribute to pancreatic disease. How might aPSC be exposed to agents that subsequently activate Ca^{2+} signaling events? In experimental models of acute pancreatitis, there is considerable evidence that trypsinogen, normally inactive until cleaved by enteropeptidases in the small intestine, is converted to active trypsin within the acinar cell (Saluja *et al.*, 1999; Kruger *et al.*, 2000; Raraty *et al.*, 2000). Trypsin, as well as other cytoplasmic contents including adenine nucleotides, is likely released into the extracellular space following acinar cell damage. In addition, during episodes of pancreatitis there is increased permeability of the vasculature, exposing the pancreas to the contents of plasma (Turjanski *et al.*, 2007). It is therefore probable that during episodes of pancreatic insult the gland is exposed to PAR ligands, PDGF, and adenine

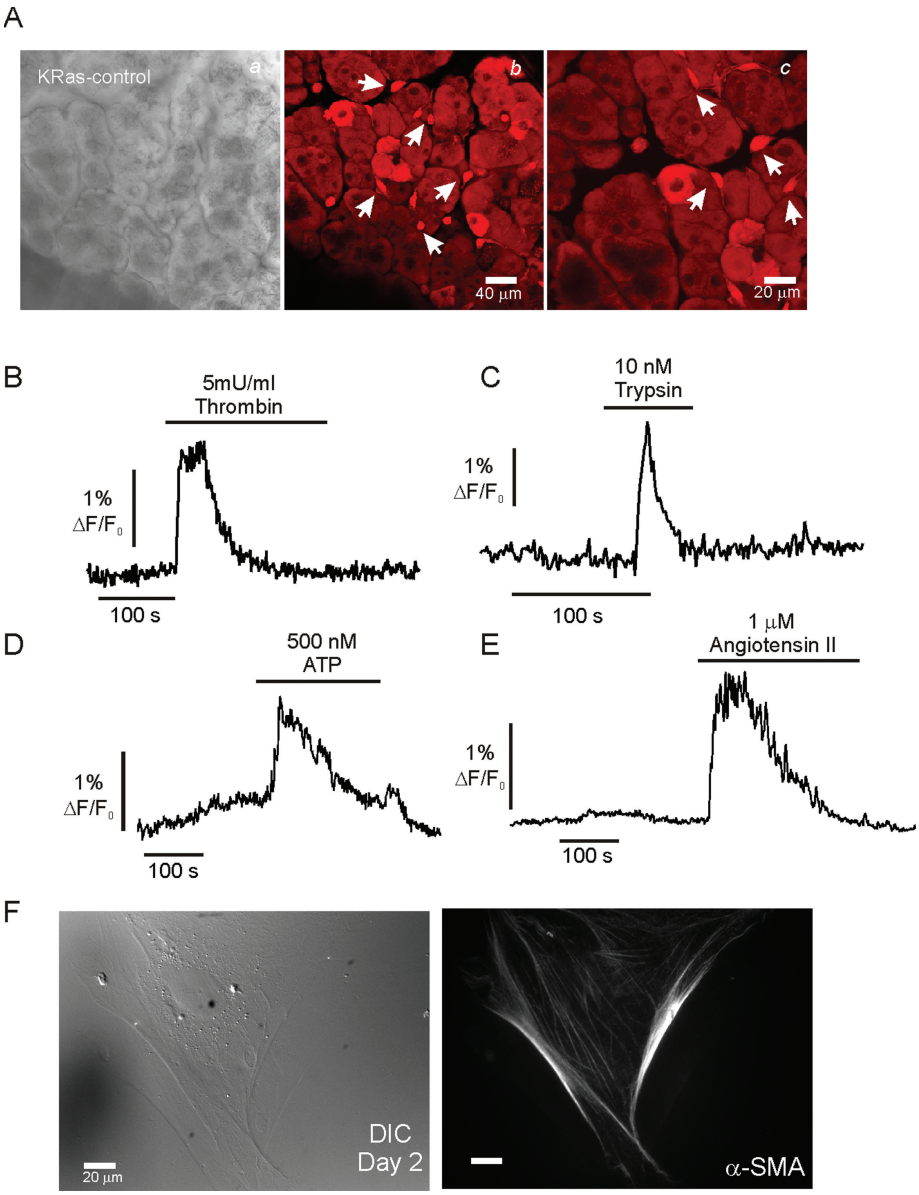

FIGURE 10: Ca^{2+} signaling in pancreatic lobules isolated from LSL-K-Ras^{G12D} mice. (A) Morphology of lobules isolated from LSL-K-Ras^{G12D} mice. (Aa) Transmitted laser light image. (Ab) Fluorescence image of lobule loaded with calcein AM at 50× and (Ac) at 100× magnification. Arrows highlight nonacinar cells with flattened morphology. (B–E) Ca^{2+} signals monitored from these cells. (B) Representative response to thrombin. (C) Representative response to trypsin. (D) Representative response to ATP. (E) Representative response to angiotensin II. (F, left) DIC image of stellate cells prepared from LSL-K-Ras^{G12D} mice on day 2 in culture. (F, right) Prominent α-SMA staining in a proportion of these cells.

nucleotides in the extracellular milieu, which, in addition to initiating gland damage, may also stimulate signaling events in both acinar cells and aPSC.

PSC Ca^{2+} signaling in lobules of pancreatic tissue: implications for disease

Elevations of $[Ca^{2+}]_i$ in PSC triggered by PAR agonists were observed in situ only from those WT animals injected with cerulein. These data are consistent with aPSC being present only following pancreatic insult. Because no direct evidence of the expression of CCK receptors on PSC was found, activation is likely the result of autocrine/paracrine effects following the production of cytokines/chemokines, growth factors, and inflammatory mediators generated following damage to acinar cells and induction of the inflammatory response (Omary *et al.*, 2007). Of note, however, despite evidence of "activation," is that no apparent increase in stellate cell numbers was observed in WT animals following cerulein treatment. Presumably, in this experimental paradigm the unchanged aPSC numbers reflect the need for an additional signal to either enhance the basal proliferation rate or overcome efficient removal of aPSC from the pancreas. This is consistent with little evidence of pancreatic fibrosis or severe morphological disruption in this model of pancreatitis (Lampel and Kern, 1977).

In contrast, in lobules isolated from LSL-K-Ras^{G12D} mice subjected to the same protocol, an approximately twofold increase in the numbers of stellate cells was observed. A majority of these cells exhibited an activated phenotype as assessed by response to PAR agonists and low [ATP], and this was accompanied by extensive expression of α-SMA and secretion of ECM, as reported previously. Interestingly, although LSL-K-Ras^{G12D} animals have been reported to have no overt phenotype until pancreatitis is induced (Guerra *et al.*, 2007), our studies provide clear evidence that PSC are primed in an activated state before insult. The primary evidence for this is that a proportion of the PSC responds to PAR agonist, and aPSC can be prepared from these animals that do not require culture for transformation. By virtue of the targeting strategy used to generate the LSL-K-Ras^{G12D} mouse (Guerra *et al.*, 2007), activation of PSC must occur as a result of the diverse signaling pathways downstream of K-Ras activation in acinar cells (Schubbert *et al.*, 2007; Kholodenko *et al.*, 2010). This "priming" of the PSC in an activated state likely promotes the proliferation of aPSC following induction of pancreatitis in this animal, resulting in a more severe manifestation of disease. It is tempting to speculate that nuclear Ca^{2+} signals initiated by agents including trypsin, thrombin, and ATP may contribute to this phenomenon. Consistent with this idea, camostat, an orally active serine protease inhibitor, has been reported to decrease pancreatic fibrosis and PSC proliferation in animal models of chronic pancreatitis (Gibo *et al.*, 2004; Emori *et al.*, 2005).

A clinical parallel may be relevant in regard to the data generated in the LSL-K-Ras^{G12D} mice. Patients with chronic pancreatitis have an increased risk of developing pancreatic ductal adenocarcinomas (PDAC) (Lowenfels *et al.*, 1993). A developing idea is that the level of Ras activity in acinar cells is an important determinant for the progression of pancreatic disease (Ji *et al.*, 2002; Guerra *et al.*, 2007). Consistent with this idea, increased K-Ras activity resulting from activating mutations is seen in virtually all tumors and ~35% of chronic pancreatitis patients (Almoguera *et al.*, 1988; Hruban *et al.*, 1993; Luttges *et al.*, 2000). Additional strong evidence to support this proposal has come from several genetic mouse models

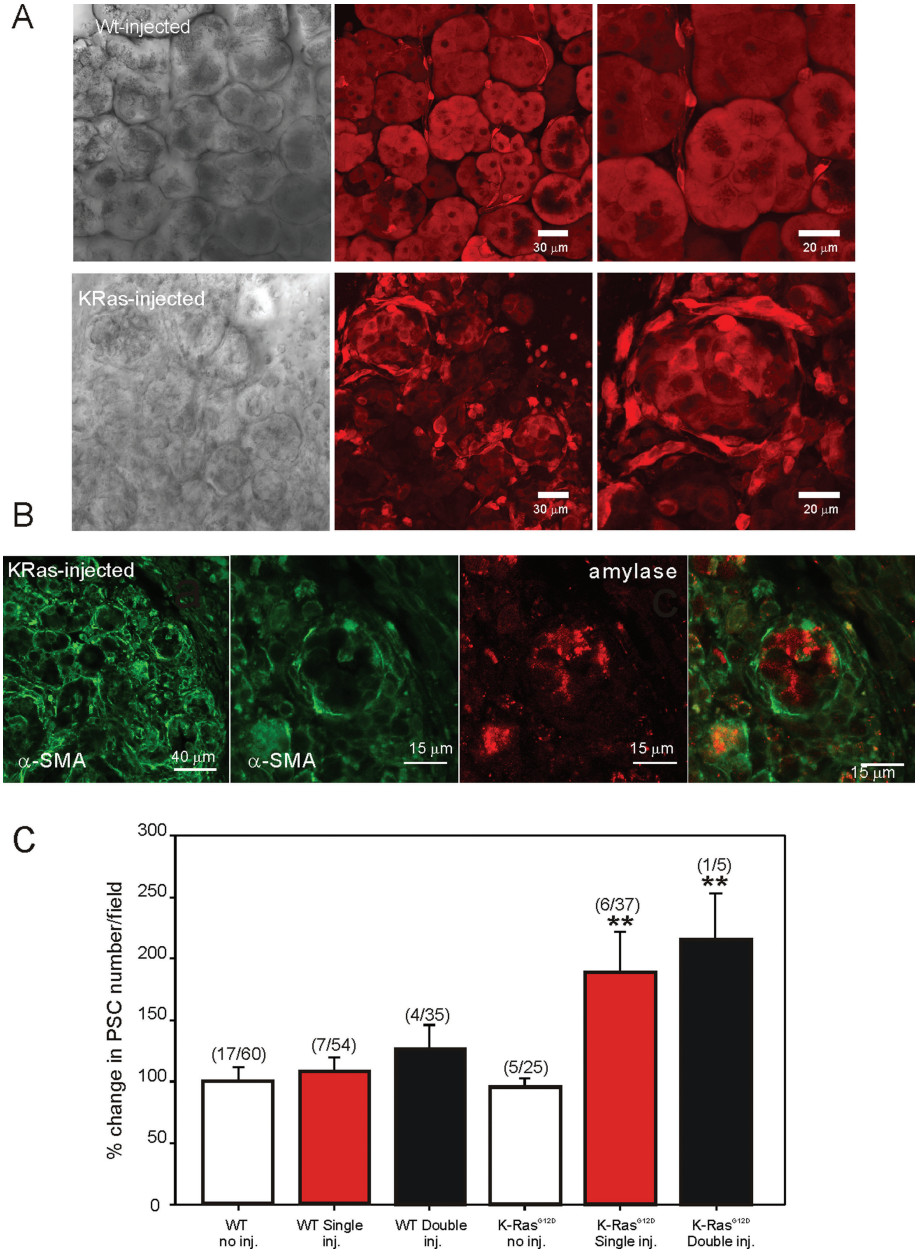

FIGURE 11: Morphology of lobules following cerulein injection. (A, top) Transmitted laser light image (left) from a lobule isolated from a WT animal injected with cerulein as detailed in *Materials and Methods*. Middle and right panels show MP excitation images of calcein fluorescence at 50× and 100× magnification, respectively, in WT lobules. (A, bottom) Transmitted laser light image (left) from a lobule isolated from a LSL-K-Ras^{G12D} animal treated with cerulein for 1 wk as detailed in *Materials and Methods*. Middle and right panels show MP excitation images of calcein fluorescence at 50× and 100× magnification, respectively, in LSL-K-Ras^{G12D} lobules. In contrast to WT animals, there is a severe disruption in acinar cell morphology together with an increase in periacinar cells. (B) Immunocytochemical staining of fixed lobules from LSL-K-Ras^{G12D} mice with antibodies against α-SMA and amylase to mark aPSC and acinar cells, respectively. Cells surrounding remnants of acinar cells are stained with α-SMA. (C) Analysis of the numbers of periacinar cells for the conditions stated. Numbers represent the number of animals/number of lobules at 50× magnification for each condition.

expressing a range of K-Ras activity, including the mice used in this study. For example, although LSL-K-Ras^{G12D} mice develop pancreatic fibrosis and precancerous lesions only after further pancreatic insult, a mouse engineered to express higher levels of K-Ras in acinar cells exhibits extensive pancreatic fibrosis and a high penetrance of PDAC without further insult (Ji *et al.*, 2002). Our data are consistent with the relatively low, but nevertheless increased, level of K-Ras activity in LSL-K-Ras^{G12D} animals effectively functioning as a "coincidence detector" that increases the likelihood of pancreatic disease; the increased K-Ras activity leads to primed aPSC that can respond to further insult, including those that lead to Ca^{2+} signaling events and aPSC proliferation. It is envisioned that further studies using a similar combination of in situ imaging and cultured PSC from these mouse models will provide additional insight into the role of PSC in pancreatic disease.

MATERIALS AND METHODS

Fluo-4 AM and Fura-2 AM were purchased from Teflabs (Austin, TX). Calcein AM was from Invitrogen (Carlsbad, CA). Ci-InsP_3 was from Axxora (San Diego, CA). α-SMA antisera and α-amylase were purchased from Sigma (St. Louis, MO); α-vimentin, α-GFAP, and α-desmin antisera were from Abcam (Cambridge, MA). Alexa Fluor 488/546–coupled secondary anti-bodies were from Invitrogen. PAR ligand peptides were from AnaSpec (San Jose, CA). Adenovirus encoding targeted parvalbumin constructs were a kind gift from Michael Nathanson (Yale University, New Haven, CT) and Fatima Leite (Federal University of Minas Gerais, Brazil).

Isolation and culture of PSCs

PSC were isolated by a modification of the method described by Apte *et al.* (1998). Briefly, pancreatic tissue from mouse (approximately 25 g) was minced with scissors and digested with 0.02% Pronase (Roche, Indianapolis, IN), 0.05% Collagenase P (Roche), and 0.1% DNAse in Gey's balanced salt solution (GBSS; Sigma Aldrich, St. Louis, MO) for 50 min. Digested tissue was then filtered through a 100-µm nylon mesh. Cells were washed and then resuspended in GBSS containing 0.3% bovine serum albumin (BSA). The cell suspension was centrifuged into a 28.7% (wt/vol) solution of Nycodenz (Sigma Aldrich) at 1400 × *g* for 20 min. The cells of interest separated into a fuzzy band just above the interface of the Nycodenz cushion and the GBSS with BSA. This band was harvested, and the cells were washed and resuspended in a mix of DMEM and F-12 medium (1:1 vol/vol) containing 10% FBS, 4 mM glutamine, and antibiotics (penicillin 100 U/ml and streptomycin 100 µg/ml). Cells were seeded at a density of 4×10^4 cells/cm^2. Viability of isolated cells was assessed by trypan blue exclusion, and cells were counted using a hemocytometer. Cells were maintained at 37°C in a humidified atmosphere of 5% CO_2/95% air. The culture medium was replaced the day after initial seeding and subsequently each 3 d. After reaching 80% confluence, the cells were released

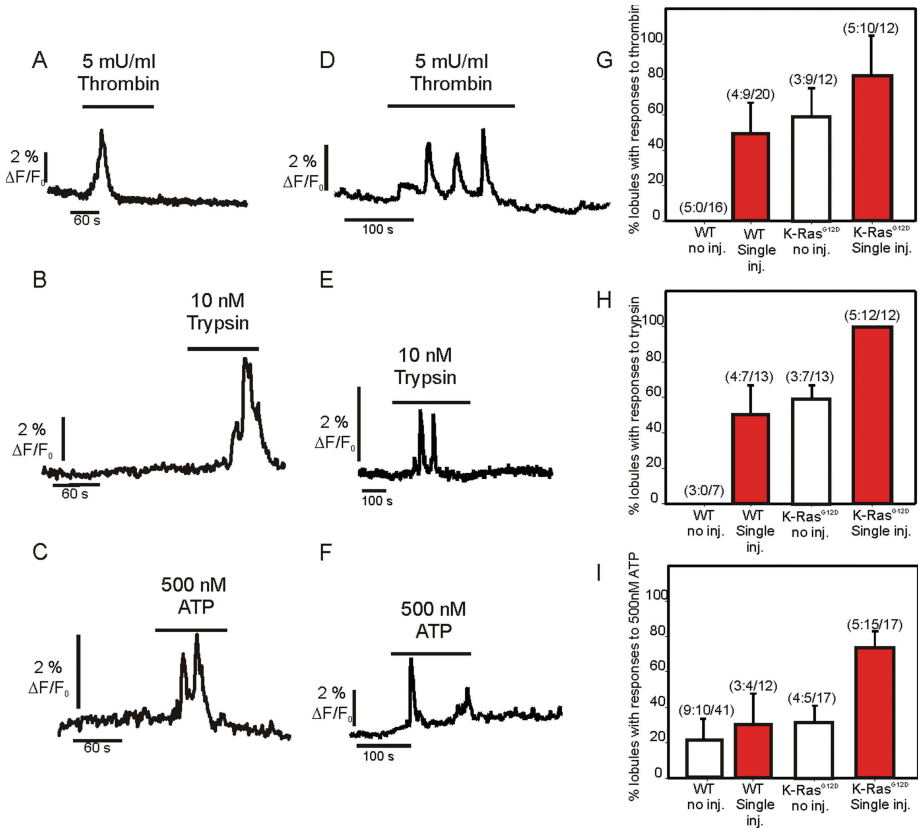

FIGURE 12: Ca^{2+} in lobules following cerulein injection. (A–C) Representative Ca^{2+} signals evoked by the indicated agonists in periacinar cells from WT animals treated with cerulein for 1 wk as detailed in *Materials and Methods*. (D–F) Representative traces from LSL-K-Ras^{G12D} animals evoked by the indicated agonists following treatment with cerulein for 1 wk. (G–I) Pooled data representing the change in responsiveness of lobules to thrombin, trypsin, and ATP following treatment with cerulein. The numbers indicate the number of animals:number of lobules for which responses were observed/total number of lobules imaged.

from the plastic by trypsinization and subcultured into 12-well plates at a density of 1×10^4 cells/well. All experiments were performed between passages 1 and 5.

Induction of pancreatic fibrosis

As previously described, mice were injected IP five times at 2-h intervals with 50 μg/kg cerulein on day 1 of the protocol followed by a single injection on days 2 through 5 (Ji *et al.*, 2009). The mice were killed on day 8 for preparation of stellate cells and lobules. In a number of experiments the protocol detailed for the first week was repeated on days 21–25 and the animals were killed on day 28. Animal procedures were approved by the University of Rochester Institutional Animal Care and Use Committee.

Immunocytochemistry and staining of lipid droplets

Immunocytochemistry in pancreatic slices was performed as previously described by Warner *et al.* (2008) for parotid gland slices. Briefly, 200-μm-thick pancreas slices were fixed with 4% paraformaldehyde. Following permeabilization and blocking, the slices were incubated overnight with the indicated primary antisera in phosphate-buffered saline–Triton (PBS-Tx) at 4°C. The slices were subsequently incubated with Alexa Fluor 488– or Alexa Fluor 546–conjugated secondary antibody at room temperature.

Cultured PSC grown on coverglass were fixed with 2% paraformaldehyde. Following permeabilization, fixed cells were incubated with appropriate polyclonal or monoclonal antisera for 1 h followed by suitable secondary antibody at room temperature (Alexa Fluor 488 or Alexa Fluor 555). α-SMA, vimentin, desmin, and GFAP were used as PSC markers. α-Amylase was used as pancreatic acinar cell marker. Fluorescence was observed on a Nikon C1 confocal microscope following excitation with 488 nm Argon laser or 563 HeNe laser with emission monitored above 560 or 600 nm, respectively. AdipoRed (Lonza, Walkersville, MD) was utilized for detection of lipid droplets. Freshly isolated PSC were seeded directly onto coverglass for fluorescence microscopy. On day 2 following isolation, cells were rinsed with PBS and incubated with 2 μl AdipoRed per ml PBS for 10 min. Fluorescence was observed on a Nikon C1 confocal microscope following excitation with 563 nm HeNe laser with emission monitored above 600 nm.

Cell proliferation assay

Cell proliferation was assessed via the incorporation of BrdU according to the manufacturer's instruction (Cell Proliferation ELISA, Roche) using a chemiluminescence-based assay detected by a plate reader equipped with a luminescence detector (Synergy 2; BioTek, Winooski, VT). Briefly, PSCs (passages 2 and 3) were seeded at a density of 3×10^4 cells/well in 96-well culture plates. After 1 d in culture, cells were infected with PV-NLS-DsRed, PV-NES-DsRed, or PV-DsRed virus at 37°C for 16 h. The cells were washed with serum-free culture medium and incubated with serum-free or 1% FBS culture. After 24 h incubation with test agents, PSC were labeled with BrdU for 3 h at 37°C. Cells were subsequently fixed and incubated with peroxidase-conjugated α-BrdU antibody and peroxidase substrate.

Ca^{2+} imaging and focal uncaging in PSC

Imaging was performed as previously described (Won and Yule, 2006; Won *et al.*, 2007). Briefly, stellate cells grown on cover glass were loaded with 2 μM fura-2 AM at room temperature for 30 min. Imaging was performed on a Nikon TE200 Inverted microscope using a 40× oil immersion objective lens coupled to a monochromator-based illumination system (TILL Photonics, Grafeling, Germany) and digital frame transfer CCD camera controlled by Vision Suite software (Betzenhauser *et al.*, 2008). Changes in Fura-2 fluorescence are presented as a change in ratio of the emitted fluorescence following excitation at 340/380 nm. For focal uncaging experiments, PSC were loaded with 4 μM Fluo-4. Focal uncaging was accomplished as previously described using a custom-built system consisting of a laser light source (90 mW, 405-nm diode) coupled through a single-mode fiber to an epifluorescence condenser (Won *et al.*, 2007). The system produces an intense, focused, and restricted area (~1.5 μm^3) of illumination at the focal plane. Brief exposure (<50 ms) provided sufficient energy to photolyse ci-$InsP_3$ without any obvious deleterious effects on the cells. Changes in Fluo-4 fluorescence are expressed as $\Delta F/F_0$, where F is the fluorescence captured at a particular time and F_0 is the mean of the initial 10 fluorescence images captured.

MP imaging in pancreatic lobules and slices

Pancreatic lobules were isolated following injection of saline beneath the capsule with a 27-gauge needle. Using a binocular dissecting scope, individual lobules < 1 mm^3 were removed with scissors. Some lobules were embedded in 3% low-temperature melting point agarose exactly, and 200-mm slices were cut using a Vibratome as previously described for parotid gland organotypic slices (Chen *et al.*, 2005). Slices were kept at room temperature in saline saturated with 95% O_2 and 5% CO_2 for 1–4 h. The lobules and slices were loaded with Fluo-4 AM for intracellular Ca^{2+} measurements (5 μM) or calcein AM for visualization of structure (5 μM) by incubation for 30–60 min. Intrinsic fluorescence was excited at the indicated wavelength and visualized in lobules not loaded with dye. Pancreatic tissue was placed in a low-volume perfusion chamber (Warner Instruments, Hamden, CT) and maintained in position by using a wire grid in a weighted metal ring. MP imaging was performed using an Olympus BX61WI upright microscope coupled to an Olympus Fluoview 1000 multiphoton/confocal (FV1000MP) microscope equipped with Spectra Physics Mai Tai (DeepSee, Santa Clara, CA) mode-locked Ti:sapphire tunable laser. Imaging was performed using a 25× water-immersion objective (XL Plan N; numeric aperture = 1.05). The laser was tuned to provide excitation at 810 nm, and emitted light was separated using a 565-nm dichroic mirror followed by emission filters HG525/50 and HQ605/50 in front of the detectors to visualize green and red emitted fluorescence, respectively. An individual plane, typically at a depth of 80–150 μm into the slice, was scanned at 1 Hz for measurement of intracellular Ca^{2+}. A Z-series through the preparation followed by analysis of a reconstructed maximum projection image was used to analyze lobule sructure.

ACKNOWLEDGMENTS

The work described was supported by National Institutes of Health grants RO1-DK05468 and RO1-DE14756 (D.I.Y.). The authors are very grateful to Jill Thompson for thorough proofreading of the manuscript and Trevor Shuttleworth for numerous helpful discussions during the course of the studies. The authors also thank Lyndee Knowlton for excellent technical support.

REFERENCES

Allbritton NL, Oancea E, Kuhn MA, Meyer T (1994). Source of nuclear calcium signals. Proc Natl Acad Sci USA 91, 12458–12462.

Almoguera C, Shibata D, Forrester K, Martin J, Arnheim N, Perucho M (1988). Most human carcinomas of the exocrine pancreas contain mutant c-K-*ras* genes. Cell 53, 549–554.

Apte MV, Haber PS, Applegate TL, Norton ID, McCaughan GW, Korsten MA, Pirola RC, Wilson JS (1998). Periacinar stellate shaped cells in rat pancreas: identification, isolation, and culture. Gut 43, 128–133.

Apte MV, Haber PS, Darby SJ, Rodgers SC, McCaughan GW, Korsten MA, Pirola RC, Wilson JS (1999). Pancreatic stellate cells are activated by proinflammatory cytokines: implications for pancreatic fibrogenesis. Gut 44, 534–541.

Apte MV *et al.* (2004). Desmoplastic reaction in pancreatic cancer: role of pancreatic stellate cells. Pancreas 29, 179–187.

Bachem MG, Schneider E, Gross H, Weidenbach H, Schmid RM, Menke A, Siech M, Beger H, Grunert A, Adler G (1998). Identification, culture, and characterization of pancreatic stellate cells in rats and humans. Gastroenterology 115, 421–432.

Berna MJ, Seiz O, Nast JF, Benten D, Blaeker M, Koch J, Lohse AW, Pace A (2010). CCK1- and CCK2-receptors are expressed on pancreatic stellate cells and induce collagen production. J Biol Chem 285, 38905–38914.

Berridge MJ, Lipp P, Bootman MD (2000). The versatility and universality of calcium signalling. Nat Rev Mol Cell Biol 1, 11–21.

Betzenhauser MJ, Wagner LE II, Won JH, Yule DI (2008). Studying isoform-specific inositol 1,4,5-trisphosphate receptor function and regulation. Methods 46, 177–182.

Bootman MD, Fearnley C, Smyrnias I, MacDonald F, Roderick HL (2009). An update on nuclear calcium signalling. J Cell Sci 122, 2337–2350.

Cardenas C, Escobar M, Garcia A, Osorio-Reich M, Hartel S, Foskett JK, Franzini-Armstrong C (2010). Visualization of inositol 1,4,5-trisphosphate receptors on the nuclear envelope outer membrane by freeze-drying and rotary shadowing for electron microscopy. J Struct Biol 171, 372–381.

Casini A, Galli A, Pignalosa P, Frulloni L, Grappone C, Milani S, Pederzoli P, Cavallini G, Surrenti C (2000). Collagen type I synthesized by pancreatic periacinar stellate cells (PSC) co-localizes with lipid peroxidation-derived aldehydes in chronic alcoholic pancreatitis. J Pathol 192, 81–89.

Chen Y, Warner JD, Yule DI, Giovannucci DR (2005). Spatiotemporal analysis of exocytosis in mouse parotid acinar cells. Am J Physiol Cell Physiol 289, C1209–1219.

Dolmetsch RE, Pajvani U, Fife K, Spotts JM, Greenberg ME (2001). Signaling to the nucleus by an L-type calcium channel-calmodulin complex through the MAP kinase pathway. Science 294, 333–339.

Echevarria W, Leite MF, Guerra MT, Zipfel WR, Nathanson MH (2003). Regulation of calcium signals in the nucleus by a nucleoplasmic reticulum. Nat Cell Biol 5, 440–446.

Eder A, Bading H (2007). Calcium signals can freely cross the nuclear envelope in hippocampal neurons: somatic calcium increases generate nuclear calcium transients. BMC Neurosci 8, 57–67.

Emori Y, Mizushima T, Matsumura N, Ochi K, Tanioka H, Shirahige A, Ichimura M, Shinji T, Koide N, Tanimoto M (2005). Camostat, an oral trypsin inhibitor, reduces pancreatic fibrosis induced by repeated administration of a superoxide dismutase inhibitor in rats. J Gastroenterol Hepatol 20, 895–899.

Fox JL, Burgstahler AD, Nathanson MH (1997). Mechanism of long-range Ca^{2+} signalling in the nucleus of isolated rat hepatocytes. Biochem J 326, 491–495.

Gibo J, Ito T, Kawabe K, Hisano T, Inoue M, Fujimori N, Oono T, Arita Y, Nawata H (2004). Camostat mesilate attenuates pancreatic fibrosis via inhibition of monocytes and pancreatic stellate cells activity. Lab Invest 85, 75–89.

Guerra C, Schuhmacher AJ, Canamero M, Grippo PJ, Verdaguer L, Perez-Gallego L, Dubus P, Sandgren EP, Barbacid M (2007). Chronic pancreatitis is essential for induction of pancreatic ductal adenocarcinoma by K-Ras oncogenes in adult mice. Cancer Cell 11, 291–302.

Haber PS, Keogh GW, Apte MV, Moran CS, Stewart NL, Crawford DH, Pirola RC, McCaughan GW, Ramm GA, Wilson JS (1999). Activation of pancreatic stellate cells in human and experimental pancreatic fibrosis. Am J Pathol 155, 1087–1095.

Hama K *et al.* (2006). Angiotensin II promotes the proliferation of activated pancreatic stellate cells by Smad7 induction through a protein kinase C pathway. Biochem Biophys Res Commun 340, 742–750.

Hennager DJ, Welsh MJ, DeLisle S (1995). Changes in either cytosolic or nucleoplasmic inositol 1,4,5-trisphosphate levels can control nuclear Ca^{2+} concentration. J Biol Chem 270, 4959–4962.

Hruban RH, van Mansfeld AD, Offerhaus GJ, van Weering DH, Allison DC, Goodman SN, Kensler TW, Bose KK, Cameron JL, Bos JL (1993). K-ras oncogene activation in adenocarcinoma of the human pancreas. A study of 82 carcinomas using a combination of mutant-enriched polymerase chain reaction analysis and allele-specific oligonucleotide hybridization. Am J Pathol 143, 545–554.

Ji B, Bi Y, Simeone D, Mortensen RM, Logsdon CD (2002). Human pancreatic acinar cells do not respond to cholecystokinin. Pharmacol Toxicol 91, 327–332.

Ji B, Tsou L, Wang H, Gaiser S, Chang DZ, Daniluk J, Bi Y, Grote T, Longnecker DS, Logsdon CD (2009). Ras activity levels control the development of pancreatic diseases. Gastroenterology 137, 1072–1082.

Kholodenko BN, Hancock JF, Kolch W (2010). Signalling ballet in space and time. Nat Rev Mol Cell Biol 11, 414–426.

Kikuta K, Masamune A, Satoh M, Suzuki N, Satoh K, Shimosegawa T (2006). Hydrogen peroxide activates activator protein-1 and mitogen-activated protein kinases in pancreatic stellate cells. Mol Cell Biochem 291, 11–20.

Kiselyov K, Wang X, Shin DM, Zang W, Muallem S (2006). Calcium signaling complexes in microdomains of polarized secretory cells. Cell Calcium 40, 451–459.

Kordes C, Sawitza I, Haussinger D (2009). Hepatic and pancreatic stellate cells in focus. Biol Chem 390, 1003–1012.

Kruger B, Albrecht E, Lerch MM (2000). The role of intracellular calcium signaling in premature protease activation and the onset of pancreatitis. Am J Pathol 157, 43–50.

Lampel M, Kern HF (1977). Acute interstitial pancreatitis in the rat induced by excessive doses of a pancreatic secretagogue. Virchows Arch 373, 97–117.
Laukkarinen JM, Weiss ER, van Acker GJ, Steer ML, Perides G (2008). Protease-activated receptor-2 exerts contrasting model-specific effects on acute experimental pancreatitis. J Biol Chem 283, 20703–20712.
Lipp P, Thomas D, Berridge MJ, Bootman MD (1997). Nuclear calcium signalling by individual cytoplasmic calcium puffs. EMBO J 16, 7166–7173.
Lowenfels AB, Maisonneuve P, Cavallini G, Ammann RW, Lankisch PG, Andersen JR, Dimagno EP, Andren-Sandberg A, Domellof L (1993). Pancreatitis and the risk of pancreatic cancer. International Pancreatitis Study Group. New Engl J Med 328, 1433–1437.
Luttenberger T, Schmid-Kotsas A, Menke A, Siech M, Beger H, Adler G, Grunert A, Bachem MG (2000). Platelet-derived growth factors stimulate proliferation and extracellular matrix synthesis of pancreatic stellate cells: implications in pathogenesis of pancreas fibrosis. Lab Invest 80, 47–55.
Luttges J, Diederichs A, Menke MA, Vogel I, Kremer B, Kloppel G (2000). Ductal lesions in patients with chronic pancreatitis show K-*ras* mutations in a frequency similar to that in the normal pancreas and lack nuclear immunoreactivity for p53. Cancer 88, 2495–2504.
Masamune A, Kikuta K, Satoh M, Suzuki N, Shimosegawa T (2005). Protease-activated receptor-2-mediated proliferation and collagen production of rat pancreatic stellate cells. J Pharmacol Exp Ther 312, 651–658.
Masamune A, Kikuta K, Suzuki N, Satoh M, Satoh K, Shimosegawa T (2004). A c-Jun NH_2-terminal kinase inhibitor SP600125 (anthra[1,9-*cd*] pyrazole-6 (*2H*)-one) blocks activation of pancreatic stellate cells. J Pharmacol Exp Ther 310, 520–527.
Mellstrom B, Savignac M, Gomez-Villafuertes R, Naranjo JR (2008). Ca^{2+}-operated transcriptional networks: molecular mechanisms and in vivo models. Physiol Rev 88, 421–449.
Namkung W, Han W, Luo X, Muallem S, Cho KH, Kim KH, Lee MG (2004). Protease-activated receptor 2 exerts local protection and mediates some systemic complications in acute pancreatitis. Gastroenterology 126, 1844–1859.
Ohnishi H *et al*. (2004). Distinct roles of Smad2-, Smad3-, and ERK-dependent pathways in transforming growth factor-β_1 regulation of pancreatic stellate cellular functions. J Biol Chem 279, 8873–8878.
Omary MB, Lugea A, Lowe AW, Pandol SJ (2007). The pancreatic stellate cell: a star on the rise in pancreatic diseases. J Clin Invest 117, 50–59.
Petersen OH, Tepikin AV (2008). Polarized calcium signaling in exocrine gland cells. Annu Rev Physiol 70, 273–299.
Phillips PA *et al*. (2010). Pancreatic stellate cells produce acetylcholine and may play a role in pancreatic exocrine secretion. Proc Natl Acad Sci USA 107, 17397–17402.
Pusl T, Wu JJ, Zimmerman TL, Zhang L, Ehrlich BE, Berchtold MW, Hoek JB, Karpen SJ, Nathanson MH, Bennett AM (2002). Epidermal growth factor-mediated activation of the ETS domain transcription factor Elk-1 requires nuclear calcium. J Biol Chem 277, 27517–27527.
Raraty M, Ward J, Erdemli G, Vaillant C, Neoptolemos JP, Sutton R, Petersen OH (2000). Calcium-dependent enzyme activation and vacuole formation in the apical granular region of pancreatic acinar cells. Proc Natl Acad Sci USA 97, 13126–13131.
Rodrigues MA, Gomes DA, Leite MF, Grant W, Zhang L, Lam W, Cheng YC, Bennett AM, Nathanson MH (2007). Nucleoplasmic calcium is required for cell proliferation. J Biol Chem 282, 17061–17068.
Saluja AK, Bhagat L, Lee HS, Bhatia M, Frossard JL, Steer ML (1999). Secretagogue-induced digestive enzyme activation and cell injury in rat pancreatic acini. Am J Phys 276, G835–842.
Schubbert S, Shannon K, Bollag G (2007). Hyperactive Ras in developmental disorders and cancer. Nat Rev 7, 295–308.
Shek FW *et al*. (2002). Expression of transforming growth factor-β1 by pancreatic stellate cells and its implications for matrix secretion and turnover in chronic pancreatitis. Am J Pathol 160, 1787–1798.
Soh UJ, Dores MR, Chen B, Trejo J (2010), Signal transduction by protease-activated receptors. Br J Pharmacol 160, 191–203.
Soliman EM, Rodrigues MA, Gomes DA, Sheung N, Yu J, Amaya MJ, Nathanson MH, Dranoff JA (2009). Intracellular calcium signals regulate growth of hepatic stellate cells via specific effects on cell cycle progression. Cell Calcium 45, 284–292.
Sutton R, Criddle D, Raraty MG, Tepikin A, Neoptolemos JP, Petersen OH (2003). Signal transduction, calcium and acute pancreatitis. Pancreatology 3, 497–505.
Turjanski AG, Vaque JP, Gutkind JS (2007). MAP kinases and the control of nuclear events. Oncogene 26, 3240–3253.
Wake K (1980). Perisinusoidal stellate cells (fat-storing cells, interstitial cells, lipocytes), their related structure in and around the liver sinusoids, and vitamin A-storing cells in extrahepatic organs. Int Rev Cytol 66, 303–353.
Warner JD, Peters CG, Saunders R, Won JH, Betzenhauser MJ, Gunning WT III, Yule DI, Giovannucci DR (2008). Visualizing form and function in organotypic slices of the adult mouse parotid gland. Am J Physiol Gastrointest Liver Physiol 295, G629–640.
Williams JA, and Yule, DI (2006). Stimulus-secretion coupling in pancreatic acinar cells. In: Physiology of the Gastrointestinal Tract, ed. ELR Johnson, San Diego, CA: Academic Press,1337–1369.
Won JH, Cottrell WJ, Foster TH, Yule DI (2007). Ca^{2+} release dynamics in parotid and pancreatic exocrine acinar cells evoked by spatially limited flash photolysis. Am J Phys 293, G1166–1177.
Won JH, Yule DI (2006). Measurement of Ca^{2+} signaling dynamics in exocrine cells with total internal reflection microscopy. Am J Physiol Gastrointest Liver Physiol 291, G146–155.
Zipfel WR, Williams RM, Christie R, Nikitin AY, Hyman BT, Webb WW (2003). Live tissue intrinsic emission microscopy using multiphoton-excited native fluorescence and second harmonic generation. Proc Natl Acad Sci USA 100, 7075–7080.